



Review

Natural and Synthetic Polymer Fillers for Applications in 3D Printing—FDM Technology Area

Bogna Sztorch ¹, Dariusz Brząkański ², Daria Pakuła ², Miłosz Frydrych ², Zdeno Špitalský ³  and Robert E. Przekop ^{1,*} 

¹ Centre for Advanced Technologies, Adam Mickiewicz University in Poznań, 10 Uniwersytetu Poznańskiego, 61-614 Poznań, Poland

² Faculty of Chemistry, Adam Mickiewicz University in Poznań, 8 Uniwersytetu Poznańskiego, 61-614 Poznań, Poland

³ Polymer Institute, Slovak Academy of Sciences, Dúbravská cesta 9, 845 41 Bratislava, Slovakia

* Correspondence: rprzekop@amu.edu.pl or r.przekop@gmail.com

Abstract: This publication summarises the current state of knowledge and technology on the possibilities and limitations of using mineral and synthetic fillers in the field of 3D printing of thermoplastics. FDM technology can be perceived as a miniaturised variation of conventional extrusion processing (a microextrusion process). However, scaling the process down has an undoubted drawback of significantly reducing the extrudate diameter (often by a factor of ≈ 20 – 30). Therefore, the results produced under conventional extrusion processing cannot be simply translated to processes run with the application of FDM technology. With that in mind, discussing the latest findings in composite materials preparation and application in FDM 3D printing was necessary.

Keywords: FDM; filament; thermoplastic; composite; additive manufacturing; particles; nanofiller; fibers; fibres; micro extrusion



Citation: Sztorch, B.; Brząkański, D.; Pakuła, D.; Frydrych, M.; Špitalský, Z.; Przekop, R.E. Natural and Synthetic Polymer Fillers for Applications in 3D Printing—FDM Technology Area. *Solids* **2022**, *3*, 508–548. <https://doi.org/10.3390/solids3030034>

Academic Editor: Dino Leporini

Received: 5 August 2022

Accepted: 26 August 2022

Published: 16 September 2022

Publisher's Note: MDPI stays neutral with regard to jurisdictional claims in published maps and institutional affiliations.



Copyright: © 2022 by the authors. Licensee MDPI, Basel, Switzerland. This article is an open access article distributed under the terms and conditions of the Creative Commons Attribution (CC BY) license (<https://creativecommons.org/licenses/by/4.0/>).

1. Short Introduction about 3D Printing by FDM/FFF Technique and Role of Fillers

The principle of additive technologies involves applying the material (polymers: resin or thermoplastic polymers; ceramic paste, metal) one layer at a time until a three-dimensional object, according to the computer-designed model, is obtained. The beginning of the additive prototyping technology dates back to the second half of the 1980s, which resulted in the world's first patent on stereolithography (SLA) [1]. The fused deposition modeling (FDM) method was developed in 1989 by the Israeli–American company Stratasys, which is among the largest players in the 3D printing market. The FDM technology itself accounts for about 40% of the world market. The technology is dedicated to low-volume production; its advantage over traditional techniques such as injection molding or extrusion is the reduced waste index, lower energy consumption [2,3], and the possibility of obtaining complicated structures without the need to use additional, expensive tools [4]. In 2021, the global market for additive technologies was estimated at USD 13.84 billion. The overall growth of the 3DP market was influenced by the global COVID-19 pandemic, logistics problems and supply chain suspension. This resulted in delays or complete discontinuation of production in many companies in Europe and the world. Current projections are a cumulative annual growth rate (CAGR) of 21% between 2022 and 2030 [5]. The largest global producers and distributors in the additive techniques industry are North America (USA, Canada, Mexico), Europe (Great Britain, Germany, France, Italy, Spain), Asia (China, Japan, India), and South Africa. Additive manufacturing methods using the FDM technique bring significant benefits in rapid prototyping, structural design and object modeling. The interest in the development of additive technologies is related to the growing demand for new prototype applications in various industries such as medicine [6] and biomedicine [7], aerospace [8], automotive [9], education [10], and rapid prototyping [11].

FDM is one of the simplest and most widely used 3D printing technologies. The method uses thermoplastic polymers, heated in the printhead above their melting point and then extruded from a nozzle on a movable printer table layer by the pressure of the filament fed into the printhead by layer [12]. FDM (fused filament fabrication—FFF) technology is characterised by low complexity and the easy availability of raw materials (filaments). The most commonly used polymers in the FDM technique include: polylactide (PLA) [13,14], glycol-modified poly (ethylene terephthalate) (PET-G) [15], amorphous acrylonitrile-butadiene-styrene polymer (ABS) [14,16,17], polyamide 12 (PA12) [18] and others such as polystyrene (PS), polyethylene (PE), poly(ethylene terephthalate) (PET), polycarbonate (PC), polycaprolactone (PCL), polyetheretherketone (PEEK), nylon and thermoplastic urethane (TPU) [19].

Various auxiliary agents can be used in FDM technology to improve materials' processing and functional properties. The most frequently used functional additives include: fillers, plasticisers, pigments, lubricants, flame retardants, stabilisers and chemical modifiers of material properties. Introducing these additives into the polymer matrix positively affects their physicochemical (thermal, electrical, rheological, hydrophobic) and mechanical properties, as well as improves the aesthetic values. Using natural, mineral, or synthetic filler often reduces the price of end products, depending on the material used (see Section 3). It often positively affects mechanical and thermal properties, as well as thermal or electrical conductivity/resistivity, depending on the filler choice and target functionality [20]. The fillers used in the FDM technology can be divided into: carbon materials (carbon black, graphene, nanotubes, carbon fibres), ceramic and metal powders, glassy and fibrous fillers (renewable raw materials such as hemp, kenaf, flax, jute [21], cellulose [22], bamboo, coconut [23], and others) mainly used to reinforce the structure and improve mechanical properties; mineral ones (titanium white, mica, metal powders, graphite, talc, chalk, diatomaceous earth), characterised by thermal, chemical and UV resistance; and biofillers (coffee grounds [24], wood flour [25]).

2. Classification of the Fillers

Fillers may be divided into classes based on several criteria, including:

- Origin;
- Chemical composition;
- Shape;
- Size and aspect ratio;
- The effects they exert on the matrix material (intended function) or their price relative to the matrix polymer.

Each of these classification methods will be briefly discussed hereinafter.

Based on the origin, we can divide fillers into natural and synthetic ones (Figure 1) [26]. Natural fillers are obtained from environmental resources (raw materials) and suitable for use after the necessary steps of preparation, such as washing, milling, sieving, drying, etc. Examples are bentonite, montmorillonite, and other types of clay. Among natural fillers, biofillers take a special place, as these are the products of (micro)organisms' bioprocesses and are considered a more renewable resource [27]. Diatomite earth may be an example of, from a chemical point of view, an inorganic (mineral) biofiller (biosilica doped with compounds of several other elements). Meanwhile, plant- (kenaf, ramie) or animal-derived fibres (cotton, silk) are organic biofiller. Synthetic fillers are products of either material synthesis or heavy chemical processing of raw materials, such as metal ores or biomaterials. The first group is represented by precipitated calcium carbonate or precipitated silica, while the latter is by TiO₂ produced via the sulfate process or synthetic silk, e.g., from the viscose method.

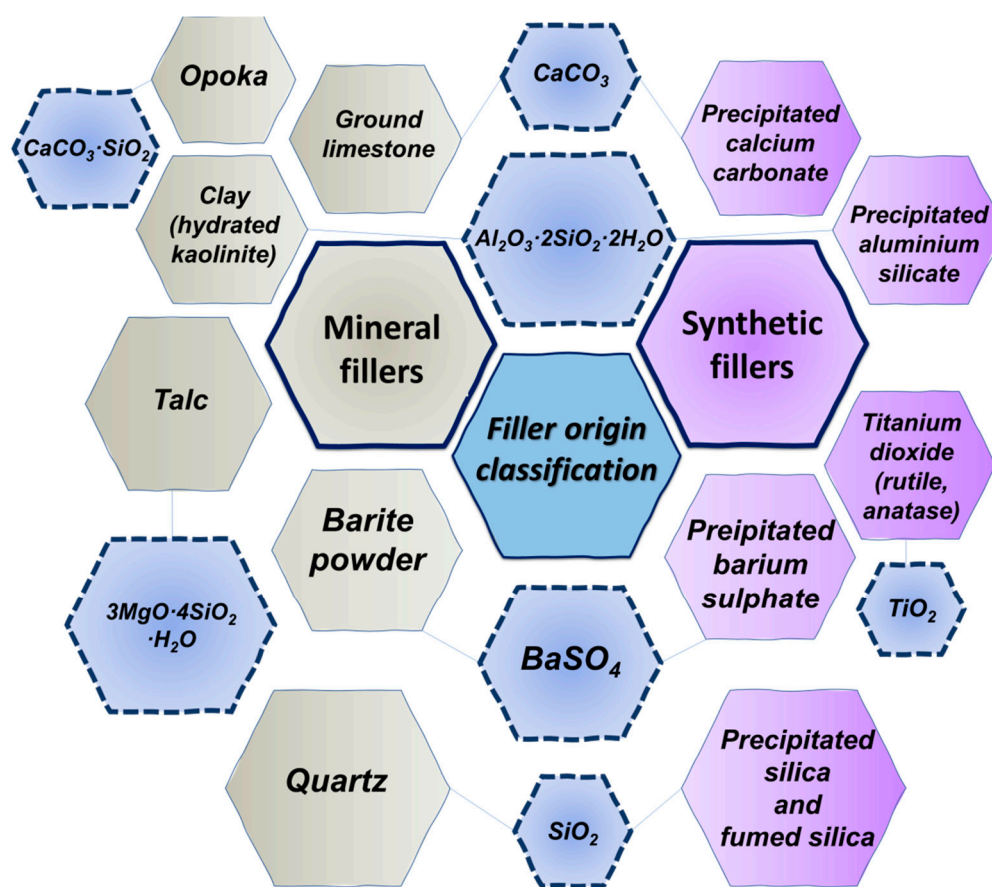


Figure 1. The division of fillers according to the origin of the material (thick frame) with examples (thin frame) and chemical formulas (dotted line).

Based on the composition, fillers can be divided into organic and inorganic types [28]. As it may be perceived as intuitive, inorganic fillers are composed of the subgroups of oxides (TiO_2 , Fe_3O_4), hydroxides ($\text{Al}(\text{OH})_3$, $\text{Mg}(\text{OH})_2$), salts (CaCO_3 , BaSO_4 , BaTiO_3), metals (boron, steel), and silicates (talc, mica). On the other hand, organic ones are represented by natural (cellulose, kenaf, ramie, silk) polymers, of which many are characterised by intrinsic fibrillar structure, and synthetic ones, such as polyamide or polyester. They are used to produce fibres and sheets for fabricating fibre-reinforced thermoplastics or laminated objects. Silicone resins also fall into this group, allowing for the control of the dynamic mechanical properties of composites, such as loss modulus or loss factor. Interestingly enough, carbon fillers (carbon fibres, graphite fibres and flakes, CNTs) are also considered organic fillers in composites engineering, despite being considered inorganic carbon materials in some other fields [29].

Depending on the size of the filler, fillers may be divided as presented in Figure 2, which comes from the classification by Bayne and Heymann for dental composite systems [30].

Wypych provided a detailed breakdown of the number of fillers falling into each size category [31]. However, it should be noted that virtually no filler of practical application is of one specific size; therefore, in the plastics industry, a common characteristic of a given filler is its size distribution, which quantitatively represents the share of particles of each size in the material's sample [32]. Another common practice is to provide the critical particle size diameters, such as d_{50} , where particle size is sorted in ascending order and the value is given when a cumulative percentage of the sample reaches 50%; in other words, it is a median of the particle size. In the same manner, d_{10} or d_{90} parameters are usually provided. However, particle size may be represented by a single (median) or a set of individual values, as mentioned above, only in a case where the filler particles have even

shapes, such as spherical or cubical. In other cases, more parameters are required. This leads to another criterion of classification, which is the filler shape.

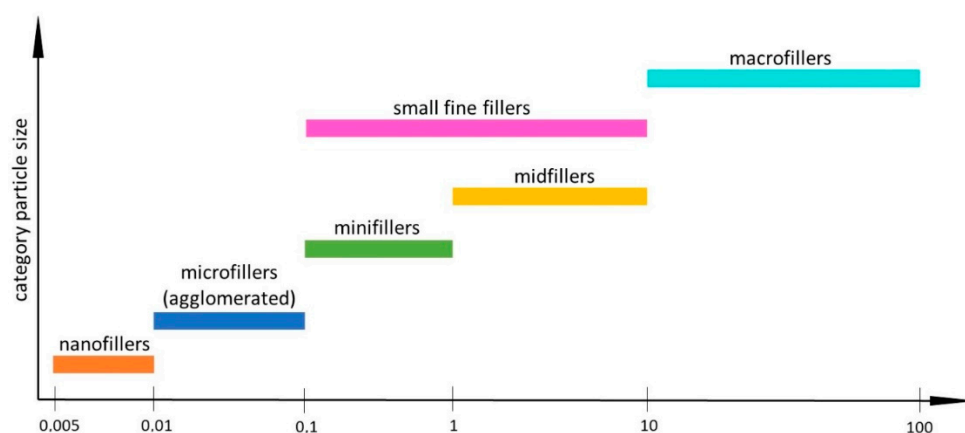


Figure 2. Filler size categories by Bayne and Heymann.

Considering that the filler is not completely random in shape (which is one of the possible shapes per se), fillers may be classified into subgroups that define different shapes, yet share a similar aspect ratio (AR), which is critical from the point of view of the mechanical reinforcing action, light reflectance/scattering properties, anisotropy effects, or melt rheology they exert on the composites they will produce among introduction into the matrix polymer. On this basis, we can distinguish the following filler shapes (Figure 3) [28]:

- Particulate: spherical, cubical, and others of $AR \approx 1$ (calcite, spherical silica);
- Blocks of AR up to ≈ 4 (barite);
- Plates of AR 4–30 (kaolin, talc);
- Flakes of AR 50–200 (aluminium, mica, graphite, montmorillonite);
- Nanosheets of $AR > 1000$ (boron nitride, graphene) [33,34];
- Fibres, nanotubes, nanowires, nanorods, nanowhiskers; AR of 20–1000+ (glass fibres, basalt fibres, carbon nanotubes Ag nanowires, TiO_2 nanorods, cellulose nanowhiskers) [35];
- Other, complex shapes, including porous and mesoporous powders, urchin-like hydroxyapatite powder, nanocluster powders, tetrapod-like whiskers, core-sheath fibres, or microcapsules [36].

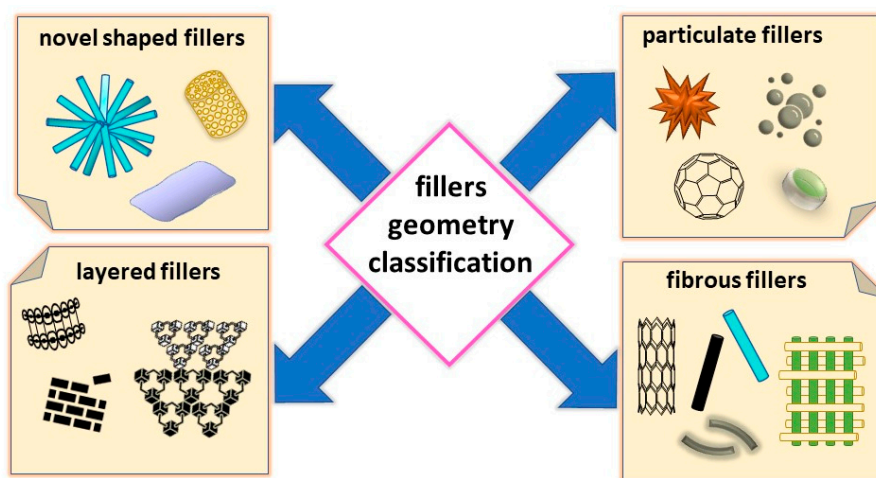


Figure 3. Different shapes of the filler applied in polymer composite design and fabrication.

The filler shape may be due to its intrinsic characteristics, where filler processing and pretreatment covers only its purification and milling/deagglomeration (natural fillers, such as talc, plant fibres), a result of the heavy processing and chemical treatment of natural material to structure it in order to obtain the desired properties, such as particle size, aspect ratio, or surface physicochemistry (nanoclays, cellulose (nano)fibrils). This is a somewhat controllable outcome, of processing conditions when preparing synthetic fillers (TiO_2 nanoparticles via sulphate or chloride process, fumed silica), or an effect of thorough nanoengineering design (nanowhiskers, carbon nanotubes).

Fillers may serve one of several roles in the composite they are applied in, and always change several characteristics of the polymer matrix they have been introduced into. The common functions of the fillers are (Figure 4) [31,33,37]:

- Mechanical reinforcement of the polymer matrix (increasing Young's modulus, tensile strength, toughness, impact resistance, abrasion resistance, hardness);
- Improving thermal and thermomechanical behaviour (increasing glass transition temperature and heat deflection/softening temperature, storage modulus or damping factor, reducing thermal conductivity);
- Reducing heat expansion coefficient or warping effect;
- Improving insulating properties (increasing breakdown strength or modifying dielectric constant), or conductive properties (conductive fillers);
- Modifying gas permeability/barrier properties;
- Inducing polymer crystallisation;
- Reducing polymer flammability;
- Modifying melt rheology;
- Modifying surface properties (roughness, hydrophobicity);
- Improving UV and weathering resistance;
- Adding colour or opacity.

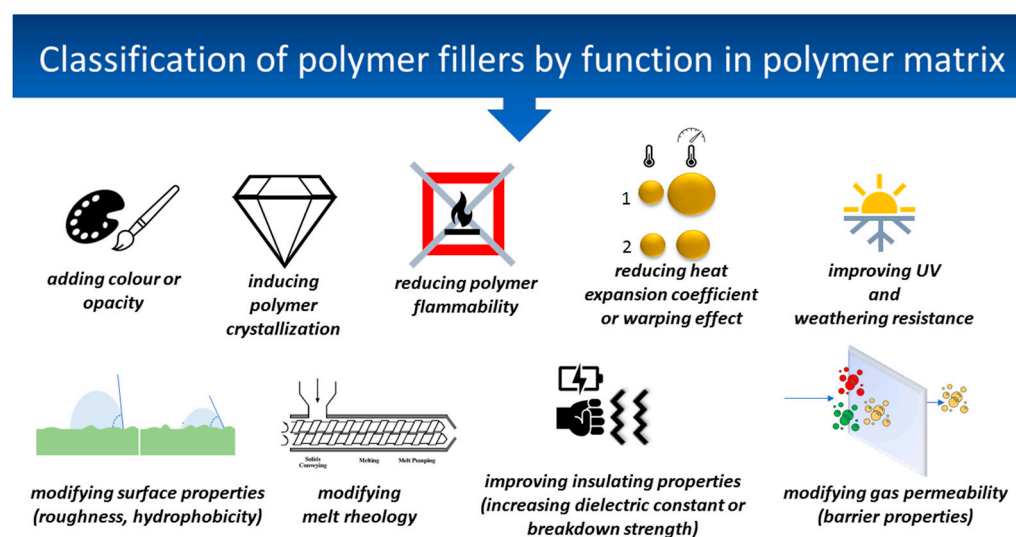


Figure 4. Different functions of fillers in polymer composites.

Fillers designed to fulfil the above-mentioned roles are often called functional fillers. Finally, a critical aspect of the filler application is its price in relation to the matrix polymer and the overall process economy when producing a chosen composite. If the main application thereof is to reduce the fabrication price of the resulting product or reduce the polymer consumption and all the other effects are considered secondary, such material will be referred to as an extender [31].

3. Statistical Presentation of the Application of Fillers in Materials for 3D Printing Based on the SCOPUS Database

The number of publications on fillers in plastics for 3D printing has grown intensively in recent years. Based on Scopus database analysis, one can see a rapid growth in 2016 (Figure 5). In the years 2004–2015, the number of publications found with the keywords ‘filler’, ‘fillers’, and ‘3D printing’ is 20, while in 2016 alone this number is 23, which shows a breakthrough moment for research related to fillers in 3D printing materials. This growing trend is related to the development of additive technologies, and thus the search for new solutions that will guarantee the improvement of the physicochemical properties of materials while reducing production costs. The total number of scientific articles in the period 2004–2022 with the keywords ‘filler’, ‘3D printing’ was 865 (including ‘filler’ and ‘FDM’-214 articles; ‘filler’ and ‘FFF’-80 articles).

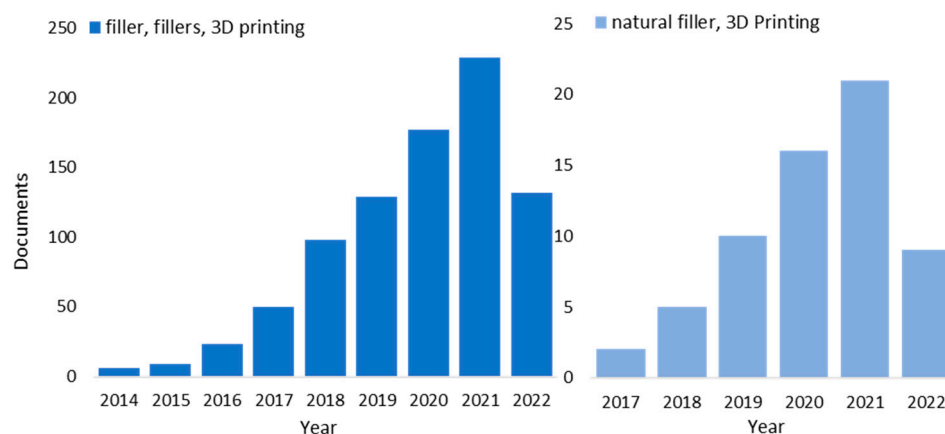


Figure 5. Scopus key words: filler, fillers, 3D printing; natural filler, 3D printing.

For both synthetic and natural fillers, the number of scientific articles increases after 2016. In 2020 and 2021, the sum of publications according to the keywords ‘natural filler’ with ‘3D printing’, and ‘mineral filler’ with ‘3D printing’ is 54, while for the keywords ‘synthetic filler’ and ‘3D printing’ the total is 14. From the obtained data, it can be seen that the number of articles describing natural fillers is 285% higher than for synthetic fillers. This shows the current trends in both science and economy, which focus on sustainable development, green economy, and green chemistry. As a result, looking for solutions based, among others, on waste- or by-products that can be used as natural fillers for plastics is a continuous trend.

4. Mineral and Natural Fillers in 3D Printing Thermoplastics

4.1. Diatoms

One group of natural fillers that are still gaining in popularity are diatoms. They are single-celled eukaryotes belonging to one of the most numerous groups of algae. Their silica shells make them peculiar, having unique ordered shapes impossible to recreate with the help of structures produced by engineering methods [38]. In addition, they are characterised by high porosity, non-flammability, low thermal conductivity, odorlessness, low moisture level, and resistance to acids [39].

The first literature reports on the use of diatoms in the FDM printing technique are attributed to Aggarwal et al. [40], who used them as a filler for PLA matrix. The obtained results showed a slight deterioration in the mechanical properties; however, the consumption of PLA was reduced by approx. 10%, while using a fraction of the production costs. The phenomenon of matrix nucleation in the presence of diatomaceous earth was also characterised. Moreover, by designing and obtaining spatial structures containing diatomaceous earth protruding from the printed object, it allowed the immobilisation of chemicals and imparting of surface properties (e.g., antibacterial, antiviral).

Examples of research using diatoms as a filler in 3D printing are the works of R. Han et al. [41,42]. These works are focused on finding applications of composites consisting of poly(DL-lactide-co-glycolide), PDLGA, with diatoms in tissue engineering. The tests showed an increase in the compressive strength of the obtained material. Additionally, the degradation of the material was compared, which showed that its modification with diatoms improves the durability of the composite. Thermal degradation also indicated a similar relationship—diatoms inhibited the thermal degradation of PDLGA. These studies confirmed the potential application of the composite as a bone-filling additive in 3D-printed scaffolds.

Dobrosielska et al., in her work, focused on the influence of diatom fraction size on the mechanical and functional properties of PLA composites intended for and tested under 3D printing conditions [43]. The obtained composites, as in the previous works, were characterised by improved thermal stability and increased mechanical strength. It was also found that the addition of a filler to the material causes the material to have higher melt flow. Due to the fraction used, different properties of the final composite were obtained. The diatom fraction $<40\text{ }\mu\text{m}$ had higher hydrophobicity, and the conditioning of samples in water resulted in an improvement in mechanical and rheological parameters. Higher mesh fraction showed greater thermal stability and tensile strength. Such composites are an emerging subject in the area of biocomposites material research and, therefore, there are not many reports in the literature at the moment.

4.2. Calcite

Calcite is the most thermodynamically stable anhydrous crystalline polymorph of calcium carbonate [44]. Due to its properties such as biological passivity, low toxicity, and good dispersion in the polymer matrix, CaCO_3 has been used in composites [45,46].

The use of calcite as a polymer filler for 3D printing is known in the literature. An example of such work is [47], who used CaCO_3 and $\text{Ca}_3(\text{PO}_4)_2$ as an addition to the composite scaffold structures produced by the FDM technique, in the field of tissue engineering. The obtained results show that with proper loading, the rate of polymer degradation can be controlled, which is important when using it during bone tissue regeneration.

CaCO_3 in a polypropylene matrix has been studied exhaustively. The filler imparts a significant reduction in the shrinkage of the printed material [48]. Other studies on the same matrix focused on the use of different anhydrous crystalline CaCO_3 polymorphs and on determining their properties [49]. It was shown that in the polypropylene matrix, only the addition of aragonite showed an improvement in mechanical properties, that is, tensile stress, by 12%.

This is in line with other data from the literature, which suggest that aragonite has a better effect on mechanical properties as a filler in polyvinyl chloride or polypropylene than calcite [50]. The remaining types of calcium carbonate either did not cause major changes in properties or worsened them. The research [51,52] showed an increase in Young's modulus, tensile strength, and tensile yield strength when using calcite nanoparticles in a PP matrix.

An example of research examining the influence of calcite on the tribological properties of polymers is the work of Sudeepan, J. et al. [53], where ABS was used as the matrix. It has been shown that the addition of 5% CaCO_3 while adjusting the appropriate process parameters (35N load, 120 rpm speed) improves the tribological properties by more than 70% compared to the reference sample.

The work of Kotlarz et al. [54] focuses on the use of three-component composites consisting of a PLGA matrix, poly(2-oxazoline) amphiphilic polymer, and CaCO_3 filler as scaffolds. Homogeneous printable composites were obtained, which contained as much as 30% of the filler in the composition. CaCO_3 and the amphiphilic polymer showed a synergistic effect on the wettability of the produced scaffolds. Moreover, the mineral addition in the degradation process caused the formation of micropores, which accelerated the degradation of the material. The novelty is that the obtained scaffolds with potential application in tissue engineering are manufactured in a one-step process.

Composites used in additive techniques consisting of PLA and CaCO₃ matrix were the subject of several scientific papers [55–58]. Mostly, the applications were limited as a substitution of complex bone defects or scaffolds in tissue engineering [59–61]. The obtained composites were characterised by the easier thermoforming of the material, a change in surface properties and in mechanical parameters compared to neat PLA—they were more brittle and stiff.

4.3. Natural Fibres

4.3.1. General Considerations

Natural fibres' use in additive manufacturing technologies for green composites has been discussed previously in several other reviews, including recent ones, e.g., of Wang [62], Shanmugam [63], Subramaniyan [64], Muthe [65], Khalifa [66], Suárez [67], Mazzanti [4], Rajak [68], Mohan [69], Ilyas [70], Badgar [71], Wasti [72], or chapters by Velu et al. [73], Murawski et al. [74], and Gharde et al. [75]. Some reviews are specifically focused on the 3D printing of natural fibre-reinforced composites, that is, by Le Duigou [76], Zhao [77], Balla [78], Li [79], Tonk [80], Deb [81], Ganguly [82], Koppaarthi [83], Mangat [84], Sekar [85], Mazzanti [86], Suriani [87], Shahinur [88], Rajendran Royan [89], Ahmed [90], Aida [91], Devarajan [92], Lee [21], and Rajeshkumar [93]. Therefore, due to the detailed exploration of this subject, only the most recent works will be discussed to provide an up-to-date review on natural fibres in FDM.

Natural fibres are commonly derived from plant matter, including wood, straws, husks, kernels, and various weeds, and falling into a group of lignocellulosic biomass exhibiting a significant variability in terms of structure and quantitative composition of cellulose, hemicellulose and lignin compounds comprising this group [94]. Popular natural fibres commonly used or tested as fillers are, among others, flax, jute, kenaf, bamboo, coir, cotton, harakeke or hemp, in addition to various wood-derived fibres. The present results show that the application of natural fibres as fillers for FDM printing technology provides satisfactory, reproducible results, although long-term part performance is still a challenge.

Mastura et al. have performed computational analysis by integrating the Analytic Hierarchy Process and Analytic Network Process, comparing several natural fibres and assessing them on the basis of criteria such as production rate, raw cost, density, mechanical parameters, or cellulose/hemicellulose/Lignin content [95]. In conclusion, by the model applied for the study, flax was found to be the most promising material, followed by kenaf and sisal.

4.3.2. PLA-Based Composites

Duigou, Fruleux et al. investigated the water- and moisture-induced shape-change properties of PLA-, PBS-, PBSA-, and PBAT-based composites reinforced with continuous flax fibre, showing an example of novel Hygromorph biocomposites (HBC) [96,97]. The authors reported a relationship between matrix stiffness and composite hygroscopic strain to be a linear decreasing trend. The shape change was an effect of the filler fibre expansion caused by water uptake. Duigui et al. also provided optimisation study on 3D printing parameters for continuous flax fibre-reinforced PLA composites, including layer height, interfilament distance, number of trips, number of layers, and their relationship with the final printing accuracy, mechanical parameters, and microstructure [98].

Stoof et al. tested hemp and harakeke fibres as reinforcing fillers for PLA composites at 0–30% loading [99]. Both types of fibres were alkali-treated at elevated temperatures of 160 °C and 170 °C, respectively (for harakeke, with an addition of sodium sulphite). Both fillers' addition resulted with decreasing tensile strength at higher loadings, especially hemp, and increasing Young's modulus. Harakeke was found to be a more effective reinforcing material; however, for both types of fibres, high filler loading resulted in extrusion and 3D printing issues, such as die blockage, printed object defects, and poor layer-to-layer adhesion.

Yaguchi et al. developed a machine setup for the direct application of continuous natural fibres under conditions of FDM printing, allowing for the use of standard printing filament, while producing composite extrudate in situ [100]. They presented the technology using PLA as the matrix and hemp fibres as the reinforcing phase. Additionally, ageing studies under UV irradiation, moisture, and simulated soil composting conditions were performed. Interestingly, the PLA used for the study, as well as the composites made thereof, showed little-to-no degradation under the tested conditions after an initial stage. Cai et al. also used a setup for introducing continuous fibres and used ramie fibres (called, in their work, in-situ impregnation 3D printing technique), also utilising machine learning methodology to refine the printing conditions towards obtaining satisfactory dynamic strength of the objects and link the printing parameters, especially layer thickness and hatch spacing, with the objects' strength characteristics [101]. An increase in layer thickness caused an increase in void content and reduced the sample strength, while reducing layer thickness and hatch spacing resulted in increased fibre content in the composite and its higher dynamic strength.

Regalla et al. reported the analysis of application of PLA reinforced with carbon fibres, jute fibres, and coir (coconut) fibres for additive manufacturing of sockets for below-knee amputation prosthetics [102]. Natural fibres provided a small increase in the composites' tensile properties, significantly smaller, however, than carbon fibres. Finite element static loading simulation allowed for correct prediction of the stress fracture site in the element. Jamadi et al. produced PLA composites with untreated and chemically treated kenaf fibres [103]. The treatment involved an alkali wash (NaOH in water solution) followed by the application of various amounts of APTES in a water-methanol solution. The results showed significant improvement of matrix-filler adhesion at up to 1% silane loading, as visible from tensile and flexural tests and SEM imaging (reduced fibre pull-out action), resulting in actual composite reinforcement.

Taborda-Rios et al. presented an optimisation process based on Tamaguchi's Design of experiments (DOEs) methodology for 20% bamboo fibre-containing PLA composites [104]. By this experimental design, deposition geometry, layer thickness, and fill density were selected as individual factors, the impact of which was assessed individually. The thorough statistical analysis allowed for the quantitative assessment of each factor; however, the most important conclusion of the study was the ineffective composite reinforcement due to lack of matrix-filler adhesion, with complete adhesive failure between the two.

Rafiee et al. described the fabrication and 3D printing of PLA composites reinforced with 0–10% of birch fibres and plasticised with 0–10% of PEG 2000 [105]. The typical problems of composite preparation were reported, especially the screw extrusion compounding, which in this case was conducted simultaneously with filament fabrication on a single-screw filament fabricating extrusion machine, which emphasises the importance of proper material compounding prior to filament extrusion, preferably on a twin-screw machine. Additionally, the authors encountered issues with the FDM process itself, including filament brittleness and nozzle clogging, as well as the process optimisation, which are the fundamental factors challenging the research involving FDM printing and are rarely expressed enough. The conclusion of the study was the filler not contributing positively to the mechanical properties of the composite, while small addition of PEG plasticised the filament, as visible from the strain-stress curves.

Dogru et al. studied the ageing effects of untreated hemp fibre-reinforced PLA 3D-printed under different infill patterns [106]. It was observed that delamination of print layers in Z axis was visible as short as one week into the ageing experiment and that, due to the lack of treatment of the fibres, inhomogeneity and matrix-filler fusion failure effects were observed in the material despite the use of a twin-screw extrusion machine. On top of that, a significant loss of tensile strength occurred over the three-week ageing study. Similarly, Kesentini et al. investigated the effects of water uptake by flax fibre-reinforced PLA composites over a 45-day period on their mechanical properties [107]. The Young's modulus and ultimate tensile strength decline was observed and visible as quickly as after

three days, while strain at rupture and loss factor were increasing, showing that the PLA degradation resulted in its plasticisation. The absorption of water by composite was stated to fit the Fick diffusion model.

Mazur et al. produced PLA composites reinforced with wood, bamboo and cork fibres under different infill ratios and studied the impact of post-process heat-induced crystallisation and saline water degradation on their characteristics [108]. It was proven that heat treatment at 85 °C induced as much as 27% crystallinity level, while as-received 3D samples showed no more than $\approx 5\%$ crystallinity, as PLA is well-known for its poor crystallisation behaviour; the treatment positively affected the tensile, flexural, and impact strength of the composites, while reducing elongation at rupture. Additionally, mechanical properties of PLA and composites thereof were provided at 80 °C to visualise the loss of structural characteristics above the T_g point of the matrix polymer.

Mangat et al. studied the effect of PLA reinforcement using silk and sheep wool [109]. The printing parameters, including the number of laminates, infill density, and raster angle, were studied in detail. On top of that, the printed structures were assessed towards biocompatibility with Madin-Darby bovine kidney epithelial fibroblast cells. The authors stated that the addition of fibres positively stimulated cell growth. The addition of reinforcing phase, however, was performed manually and done between the 3D-printed layers, resulting in a laminate structure.

Sekar et al. produced micro-perforated panels of controlled porosity from PLA/wood fibre composite for sound absorption application [110,111]. Changing the perforation volume and pore size allowed for the limited tuning of the sound absorption coefficient over the frequency range.

4.3.3. Other Polymer Matrices Reinforced with Natural Fibres

Balla et al. described composites based on Hytrel 4056 thermoplastic polyester elastomer reinforced with soybean hulls after different pretreatment procedures, including dry blending, wet shear mixing, single- and two-stage hydrolysis [112]. The acid hydrolysis procedure resulted in significant reduction of samples' porosity in terms of pore fraction and size, as well as improved the composites' toughness and increased their Young's moduli.

Ariel Leong et al. reported trials on printability of 0–10% corn husk fibre-reinforced composites utilising recycled polystyrene foam (rPS) as a feedstock matrix [113]. H_2O_2 treatment was applied to the fibres, which was proven to successfully remove lignin content. The fibre content of 2.5% caused a 38% reduction in MFI when compared to the neat rPS. Printing and layer adhesion issues both for neat rPS and the composites were observed, with 10% composition being found to be unprintable and the composite filament being brittle. The addition of the filler also negatively affected the thermal stability and tensile properties of the composites, besides elongation at rupture for 2.5% composition. Costa et al. utilised alkali treatment followed by H_2O_2 oxidation method when preparing ABS composites reinforced with pine cone fibres [114]. The XRD and FT-IR measurements confirmed removal of lignin and hemicellulose from cellulose when comparing H_2O_2 -treated samples with the raw material or alkali-treated-only samples. This procedure has resulted in the improved thermal stability of the fibres, as well as matrix-filler compatibility, as suggested by SEM imaging and material density measurements. The mechanical testing data were not provided.

Ahmad et al. prepared ABS-based composite with 5% of oil palm fibres and provided tensile and flexural characteristics of the obtained 3D-printed specimens; however, only two specimens were used per experiment [115]. The filler did not provide reinforcing action and microscopic analysis showed layer-to-layer adhesive failures on top of stress cracking of the material itself. Han et al. studied ABS/kenaf composites at 0–10% loading [116]. The materials suffered from poor layer-to-layer adhesion, which resulted in parts delamination during flexural tests, and all the systems obtained were characterised by toughness lower than that of the matrix ABS.

Balla et al. investigated soybean hull fibres after various pretreatment procedures as fillers for thermoplastic copolyester (TPC) [117]. The fibres were ground under dry and wet conditions, and either used as such or further treated by a single- or two-step sulfuric acid solution hydrolysis. The study concluded that acid hydrolysis is an effective means to promote matrix-biofiller adhesion, which in turn reduced sample porosity and increased Young's modulus; however, no significant improvement of tensile strength was observed, which, in combination with reduced elongation at rupture, translated into reduced sample toughness.

Carrete et al. proposed a methodology for recycling waste textile materials as a source of cellulose fibres and PET from drinking water bottles (unused ones) as a feedstock material for fabrication of composite filaments [118]. For the adhesion-promoting step, cellulose was first hydrolyzed in a H_2SO_4 -HCl mixture and, after neutralisation, further treated with APTES. A significant increase of impact resistance was observed, and the SEM imaging allowed for confirmation of the transition from brittle to ductile mode when comparing neat PET and modified cellulose-reinforced PET. Additionally, a two-fold increase of melt flow index was registered.

Morales et al. studied recycled polypropylene (rPP) reinforced with untreated rice husk fibres (0–10%) [119]. The material containing 10% of filler was characterised by water uptake about a magnitude of power higher than neat rPP, which is typical for NFRPs. Additionally, the water uptake caused significant swelling, which is in line with Le Duigou's findings [96]. The filler addition caused the reduction of samples' crystallinity when compared to neat rPP, especially at 5%, and, depending on printing orientation, caused significant changes to the composite mechanical properties. At 0° , all the parameters (tensile strength, elongation at rupture, Young's modulus) were decreased, while at 90° , a reinforcing action of the filler was reported, with both 5% and 10% composite providing improved toughness. The authors observed a reduced warping effect as well. They also tested cocoa bean shell fibres at 5% w/w as a filler for rPP [120]. The fibres caused a drop in material crystallinity due to amorphous lignin and hemicellulose content, not providing any nucleation to rPP. SEM imaging allowed the identification of particles fracture, filler-matrix debonding and matrix fractures as different failure mechanisms. The filler, however, reduced warping effect by 67%, while causing only minor swelling when the material was exposed to water. A significant fall of tensile properties was observed in 0° raster orientation, due to poor reinforcing action, while in 90° orientation, a small improvement was observed, showing increased layer-to-layer adhesion.

4.4. Other Natural Fillers

Other examples of natural fillers, i.e., wood flour, rice husk, cocoa shell waste, egg shell cork powder, and rachis from chicken feathers used in the processing of plastics for additive technologies are also known in the literature. They constitute, i.e., by-products or waste from various sectors of the economy. Their use in polymer composites allows the reduction of the production costs of new polymer-based materials without deteriorating the physicochemical properties, while being in line with the trend of sustainable economic development due to the reuse of waste. There are reports on using wood in various forms as a filler for plastics used in additive technologies. Examples are given on the use of wood flour in materials for 3D printing [121–123].

The first of these works describes polylactic acid (PLA) composites with 5 wt.% wood flour content. The produced material exhibited increased initial deformation resistance in comparison to neat PLA. The second work concerns the use of wood flour in another material, thermoplastic polyurethane. The conducted mechanical tests showed a decreased tensile strength with an increase in the filler content. The tensile strength showed lower values for the filler content of 20 wt.%, while they increased with filler loading above 20 wt.%. SEM and FT-IR analysis confirmed good compatibility between the filler and the matrix after modification with the EPDM-g-MAH compatibiliser, as well as higher elongation at break. Other papers also describe the effect of plasticiser additives on changes

in the properties of composites with wood-based fillers. Xie et al. studied the use of a combination of plasticisers (glycerol and tributyl citrate in various ratios). Kariz et al. investigated the influence of the wood content in the filament on the properties of 3D-printed materials. The authors obtained six filaments with a wood content from 10 wt.% to 50 wt.% in polylactide. Filaments with 10 wt.% content show an increase in tensile strength from 55 MPa to 57 MPa, but higher wood contents decreased this parameter. Material with 50 wt.% wood has achieved a tensile strength of 30 MPa. Higher wood loadings changed the surface morphology of composites. The surfaces were rougher and also had more defects and voids. The studies describe the possible use of wood in PLA, but in order to obtain better properties, the process should be optimised [124].

Le Guen et al. presented the preparation of PLA filaments with the addition of rice husk (10 wt.%) and wood powders (10 wt.%) by the twin-screw extrusion method. The biofillers have been characterised in terms of their physicochemical properties (including particle size, density, solid-state NMR, or ash content). When comparing the complex viscosity of neat PLA to the biofiller-containing compositions, the introduction of wood powder increased the complex viscosity of the compound, whereas rice husk powder decreased it. The obtained results were explained on the basis of the higher specific surface area compared to wood flour and the presence of silica in rice husks. The authors of the work noted that the mechanical properties of the materials depended on the printing direction, while the type of filler used did not significantly change the strength parameters. For example, storage modulus values at 30 °C for neat PLA printed at 0° (the longitudinal direction) was 2.66 (0.22) GPa, for PLA-wood 2.31 (0.07) GPa, and for dila PLA–rice husk 2.50 (0.15) GPa [125].

Tran et al. described the process of biofilament production based on cocoa shell waste, which is a by-product in the chocolate production industry, in a poly(ϵ -caprolactone)-PCL matrix. The authors of the study obtained composites with a waste content of up to 50%. The conducted research showed that the addition of micronised cocoa shells did not significantly change the crystal structure of the polymer and the Young's modulus. The scanning electron microscopy confirmed the very good dispersion of cocoa shells in the polymer matrix without the need to use compatibilisers or other chemical modifiers. The obtained material can potentially be used in 3D printing in home and biomedical applications [126]. Another example of the use of shells as fillers is described in the work by Girdis et al. [127]. The paper examines the use of Macadamia nut shells, a by-product of forestry and agriculture, as a potential alternative to wood polymer composite filaments. The composites consisted of 19–29 wt.% of biomass in the acrylonitrile–butadiene–styrene (ABS) matrix. Samples with 19 wt.% of macadamia shells had a higher tensile stress than commercially available wood-filled material, and were also lighter by more than 30% compared to commercial wood-filled material. However, along with the increasing amount of shells in the ABS matrix, a decrease in strength for all samples was noticeable.

Brites et al. presented the use of cork powder, which is the largest by-product of cork processing, as a natural filler for applications in 3D printing. The work compares the physicochemical properties of high-density polyethylene (HDPE) composites obtained with natural fillers, i.e., neat cork powder, as well as cork powder being a waste material obtained from the production of floor coverings, containing impurities, e.g., varnish, wood fibre, polyvinyl chloride and polyurethane. HDPE-g-MA was additionally used as a coupling agent. The research of the density shows that a larger weight amount of waste cork powder can be added to the polymer than the neat cork powder [128]. In terms of mechanical properties, all cork polymer composites (CPC) had a lower tensile strength than neat HDPE and a decrease of strain at rupture.

Sankaravel et al. investigated the properties of a PLA/egg shell biocomposite for use in the FDM technology, which could potentially be applied in tissue engineering. The filler content in PLA and the porosity of the material was up to 12 wt.% and 60%, respectively. Loading of up to 10 wt.% of the eggshell allowed for accurate printing, while the weight percent of 12% of the filler increased the brittleness of the filament. The composite materials

showed a better osteoregenerative performance in vitro with increasing egg shell content. The composite materials also had a higher compressive strength parameter (the highest value obtained for 10 wt.% of the filler), while 12 wt.% caused printing issues (nozzle clogging, poor flow). The increase in the content of eggshells allowed the reduction of the acidic reaction of PLA by changing the degradation rate and bioactivity [129].

Flores-Hernandez et al. developed a PLA-based composite reinforced with rachis from chicken feathers. The materials were characterised by the content of rachis in the range of 0.5–1 wt.% and 5–10 wt.%. Rachis was modified with NaOH and ground before being incorporated into the plastic. The thermomechanical tests carried out showed a significant improvement of the storage modulus (195%) at 1 wt.% rachis as compared to neat PLA. The analyses showed that the addition of small amounts of keratin materials improve the thermomechanical and thermal conductivity properties of the polymer [130]. Due to the increasing amount of waste in the economy, new solutions are sought that will allow for their reuse.

In the work [131] two lignocellulosic fillers were obtained from *Opuntia ficus indica* (cladodes from *Opuntia ficus indica* (OFI)) and *Posidonia oceanica* (scraps were collected on the Palermo coast), which were used to prepare PLA-based composites. The filler materials were pre-washed and ground before further processing. The research shows that it is possible to replace the polymer with 20% filler, thus reducing production costs without significantly changing processability and mechanical properties. A commonly used filler in PLA matrix is biodegradable starch, which consists of amylose and amylopectin. Due to the poor adhesion between PLA and starch, appropriate plasticisers [132,133] and chemical modifications are often explored [134]. Increasing the interactions between starch and the matrix allows the improvement of the properties of, among others, impact strength and other mechanical properties.

5. Synthetic Fillers in 3D Printing of Thermoplastics

5.1. TiO_2

Hossain et al. assessed the printability of binary blends of PLA with HDPE and multicomponent blends consisting of PLA and recycled plastics, and 1% of TiO_2 as an additive [135]. The recycled plastic comprised a mixture of several polymers, including PET, ABS, PLA, PP, HDPE, and PS. The FDM process parameters were optimised via machine learning protocol. Both the addition of TiO_2 and recycled plastics resulted in a requirement for running the process at higher temperatures (210 °C and 223 °C, respectively) when compared to neat PLA. The addition of TiO_2 caused a significant rise in the composite water uptake, from $\approx 1\%$ for the blends to 6.35% and 7.39% for TiO_2 -containing binary and multicomponent systems, respectively. In addition, the pigment presence resulted in surface imperfections of the printed samples. The non-pigmented blends showed elongation at rupture of up to 22%, superior to that of usual neat PLA; however, the addition of TiO_2 caused a large drop in this feature.

Olam et al. prepared PLA-based composites with varying amounts (0–4%) of TiO_2 and either natural or synthetic hydroxyapatite [136]. By means of SEM imaging, they observed that the addition of TiO_2 caused raster gap reduction in printed samples, and EDX analysis allowed the confirmation of the high homogeneity of the samples. Furthermore, a significant rise of glass transition temperature was observed, from 52 °C for the neat PLA up to 71 °C for the material containing 4% of TiO_2 and 1% of synthetic HA. The same material showed improved tensile properties of both the tensile strength (by $\approx 20\%$) and strain at rupture, as well.

Singh et al. developed PA6 composite filament loaded with 30% of TiO_2 [137]. The authors did not perform 3D printing experiments, but they studied in detail the twin-screw extrusion process and optimised it towards the minimal porosity of the filament surface and mechanical parameters. Furthermore, an increase of MFI from 24.6 (neat PA6) to 39 g/10 min was observed. Soundararajan et al. studied mechanical properties of PA6 composites containing 0–30% of TiO_2 [138]. Progressive increase of tensile strength and

Young's modulus were observed, as well as a decrease of elongation at rupture, when using standardised tensile dumbbells prepared by 3D printing. The composites were more resistant to tribological wear measured by pin on disc method, independently on the load applied, the wear rate being reduced by as much as 66% for 30% TiO₂ loading.

Tiwary et al. studied ABS/TiO₂ composites of 5–15 wt.% loading. Satisfactory level of tensile strength at 20.5 MPa was reported at 10% TiO₂ loading [139]. Additionally, the authors explored the photodegradability of the materials, correlating the sample mass loss with the UV source power and titanium white mass fraction. The mass loss, however, was minute, as the experiment was performed for 4 h only. Vidakis prepared ABS/TiO₂ composites (0–10% loading) and observed, under optimal conditions, an increase of tensile strength by 7% and flexural strength by 12% (at 2.5% loading), and Vickers microhardness by 6% (at 10% loading) [140]. The filler addition did not affect the thermal degradation profile of the composites at any loading. In another work by the abovementioned group, polypropylene (PP)/TiO₂ composites were studied at 0–4% filler loading [141]. Small reinforcing effects were observed under tensile and flexural load, revealing that for flexural properties, the highest (4%) loading was the most beneficial, while for tensile properties, impact resistance, and microhardness this was 2% loading. Besides 4% loading, all the samples exhibited increased damping factor ($\tan\delta$) values from the DMTA study.

Car et al. explored the applicability of various thermoplastic materials as matrices for the 3D printing of monoliths for the catalytic oxidation of volatile organic compounds (VOCs) [142]. The catalytic activity experiments were not included in the work, the investigation being focused on the composite preparation and additive manufacturing, together with basic (TGA, tensile properties) material testing. LDPE, HDPE, PETG, HIPS, ABS, PC/ABS blend Z-PCABS, ABS-based Z-ULTRAT, and thermoplastic polyester-based Z-GLASS (the last three materials being branded by Zortrax) were tested. On the basis of TGA, Z-PCABS, Z-PETG, and Z-GLASS-based systems were selected for 3D printing experiments. It was observed that, due to thermoplastic properties of the matrices used, the monoliths are suitable for photocatalysis, and not thermal oxidative catalysis, as the monoliths underwent heat deformation above 170 °C. Finally, Z-GLASS was chosen as the matrix for this purpose on the basis of its transparency, which was seen as beneficial from the point of view of photocatalysis. It was found that TiO₂ addition (in 1–10% ratio loading) does not affect the thermal stability of the composites significantly, although at the highest loadings, a decline of mechanical properties occurred.

Sevastaki et al. developed PS/TiO₂ composite photocatalysts with 20% and 40% nanoparticle loading, using recycled polystyrene [143]. The photocatalysts were then tested in a drug UV-A photodegradation study of acetaminophen (paracetamol), where three repeated runs were performed for each catalyst, allowing for the decomposition of ≈60% of the drug in each run. Similarly, Viskadourakis et al. prepared PS/TiO₂ photocatalytic scaffolds that allowed for the full degradation of methylene blue within 60 min of an experiment and showed activity under conditions of repeated reaction cycles [144]. Using a similar strategy, Sangiorgi et al. prepared photocatalytic, filter-like scaffolds containing 15 and 30% of PEI-stabilised TiO₂ nanoparticles embedded in the PLA matrix [145]. The scaffolds effectively catalysed the photodegradation of methyl orange. The impact of scaffold geometry and printing infill was also discussed. Zhou et al. developed a 3D-printed compact flow reactors from PLA containing 5% of TiO₂ as a photocatalytic phase, for water purification purposes [146]. Methylene blue and phenol were used as model molecules, and the reactors were proven to be effective under single pass and circulating flow conditions, with no apparent loss of photoactivity. The critical step in obtaining the high activity of the catalytic phase was UV-A pretreatment of the composite. Li et al. utilised aqueous-phase plasma-aided grafting method, based on cold plasma discharge, to graft TiO₂ and ZnO particles on the surface of 3D-printed PLA, following a number of different strategies: direct grafting of nanoparticles onto an activated surface (proven only feasible for ZnO); grafting of core-shell particles coated with either poly(acrylic acid) or methacrylic acid (for ZnO), or a variation of the same using vinylphosphonic acid (for TiO₂);

and grafting the unmodified particles to plasma-activated PLA surface via an intermediate phase of poly(vinylphosphonic acid) (PVPA) coating [147]. The obtained photocatalysts were then assessed towards the degradation of Rhodamine B dye as a model molecule of organic pollutants. The PVPA coating method was proven to be effective for both types of NPs, and discussed as an efficient means for grafting a high variety of inorganic particles. All the photocatalysts were proven effective, and the ZnO-based system was additionally tested in a three-run experiment with only slight reduction of the photoactivity. McQueen et al. studied the photocatalytic activity of PLA/TiO₂ composites for decomposition of 4- and 5-member polycyclic aromatic hydrocarbons (PAHs) [148]. The elimination of PAHs was quantified over the time of 6 to 24 h, and proven to undergo this via both photodegradative and photocatalytic pathways, with the latter (PLA/TiO₂ composite-assisted) being significantly faster and providing a reduction in PAHs concentration to non-detectable levels within 24 h. The effectiveness of PAHs removal was additionally demonstrated, as the photo-treated water became non-toxic to *Ceriodaphnia dubia*, a species of water fleas.

Kumar et al. proposed a methodology of multimaterial printing utilising PLA and PA6/TiO₂ materials, preparing layered composites [149]. A PA6/TiO₂ 'shell' provided improved wear resistance under pin on disc tests and increased elongation at rupture, but did not protect the PLA phase from cracking. Furthermore, void formation and debonding between the polymer phases were observed by SEM.

Nájera et al. assessed the applicability of PLA/PCL blend doped with TiO₂ of various medium particle sizes as composites for bone tissue grafts [150]. The composites did not show complete polymer melt blending, as stated from DSC analysis; however, the addition of small- and medium-sized TiO₂ particles resulted in improved mechanical properties of the composites when compared to the polymer blend, both in terms of tensile strength and elongation at rupture. A comparison with neat polymer components was not provided. The composite was characterised by biocompatibility with mouse calvarial preosteoblast cells MC3T3-E1.

Braunstaen et al. investigated the antimicrobial properties of ZnO- and TiO₂-filled PLA-based composites plasticised with poly(ethylene glycol)s (PEGs) of different molecular weights (1 kDa, 2 kDa and 10 kDa) [151]. The incorporation of TiO₂ did not affect composite thermal stability, while ZnO caused a significant drop of onset temperature (>50 °C considering T_{5%} parameter), and PEG additives caused a drop of T_g (below the measurement temperature threshold of 25 °C). PEGs addition also significantly increased strain at rupture (from ≈6% up to ≈105%), drastically reducing tensile strain and Young's modulus, however. Additionally, ZnO and TiO₂ were proven to exhibit antimicrobial properties, while PEGs did not affect the PLA biodegradability. Horst et al. verified the printability of natural oleo-gum resins as from styrax benzoin, myrrha, and olibanum as substrates for FDM-based 3D printing [152]. In addition, the materials were loaded with 10% of either TiO₂, Cu₂O or MoO₃ nanoparticles. The resins showed some antibacterial properties against *S. aureus*, *E. coli*, *P. aeruginosa*, and *C. albicans*, while the addition of any type of chosen NPs resulted in the improvement of this property.

Ding et al. assessed the applicability of PEEK-based composites with TiO₂ and Fe₂O₃ as pigmenting fillers [153]. Most of the systems produced exhibited tensile strength and modulus comparable with or higher than that of PMMA resin used as a standard for comparison, while having greatly improved flexural strength (even by three-fold) and significantly higher flexural modulus. This finding showed a potential for the practical application of such materials as dental composites. Dong et al. developed methodology for producing tissue-simulating phantoms with FDM technology, using low-melting gel wax loaded with TiO₂ and graphite as a scattering and absorbing agents, respectively [154]. The FDM system was equipped with a mixing system that allowed application of the scattering and absorbing components in a required ratio, thus providing the optical properties required to mimic the simulated tissue in a satisfactory manner. The method allowed for the 3D printing of a brain phantom on the basis of simplified MRI slice images.

Castro et al. developed high-permittivity, cyclo-olefin polymer-based (COP) composites filled with either TiO_2 , MgCaTiO_3 , or $\text{Ba}_{0.55}\text{Sr}_{0.45}\text{TiO}_3$ fillers, for application in RF/microwave devices [155,156]. The obtained composites were characterised by high (>4.5) ϵ_r parameters, and besides the case of $\text{Ba}_{0.55}\text{Sr}_{0.45}\text{TiO}_3$, very low-loss tangent $\tan\delta_d$. ABS as a matrix, on the other hand, provided less satisfactory electromagnetic characteristics.

5.2. Glass Fibres

The use of glass fibres (GF) in the composite materials industry dates back to the late 1930s. This was related to the optimisation of the commercial fibre production process for use in composite materials by Owens-Illinois Glass Company. The second event influencing the progress of glass fibre-reinforced polymers was the development by DuPont of resins that could be modified with glass fibres [157]. Currently, the most important branch of industry, using the largest amounts of glass fibres produced, is the thermal insulation market. The second most important and biggest market in terms of GF usage is the composite materials sector, in which GF is the reinforcement of polymers [158]. The development of additive techniques and the need for composite materials with better mechanical performance have made glass fibres also used in 3D printing [159].

Glass fibres are used as reinforcements in, among others, PP, ABS, PEEK, PLA, and polyamides. Shulga et al. presented the results of micro-CT analysis and mechanical tests of materials based on polypropylene (PP) reinforced with short glass fibres. The samples were printed with the FFF method in different raster orientations (90, 90 and 45, 135), with different thicknesses of the layers. The presented results show the significant influence of the orientation of the short glass fibre on the tensile strength, modulus, and stress at rupture [160].

Sodeifian et al. analysed the mechanical, rheological, and crystallinity properties of PP/GF and PP/GF composites with maleic anhydride-grafted polyolefin (POE-g-MA) as a coupling agent. PP/GF materials were characterised by high brittleness; the addition of POE-g-MA increased the flexibility of the composites. Tensile strength analysis showed that the addition of GF increases strength and modulus, while reducing flexibility. The addition of POE-g-MA increases flexibility, but lowers the ultimate tensile strength [161]. Carneiro et al. compared the properties of neat polypropylene and commercially available polypropylene reinforced with 30 wt.% of glass fibres. The composite was characterised by higher modulus and tensile strength parameters in relation to neat PP by approximately 30% and 40%, respectively [162].

Mohan Kumar et al. investigated the effect of the addition of short glass fibre on the mechanical properties of composites in the ABS matrix. The authors suggest strong interactions between the matrix and the fibres, which resulted in an increase in the Young's modulus and strength of the samples, with a simultaneous decrease in the value of elongation at break [163]. Similar results were obtained by Zhong et al. [164], who conducted a series of experiments of glass fibre-reinforced materials on an ABS matrix. The analysis showed that glass fibres (30% by weight) significantly improve the strength of the material, but significantly increase brittleness, which results in difficulties in its processing. The obtained materials could not be used for the FDM method. Only the addition of a plasticiser and compatibiliser (LLDPE) allowed for the effective use of the material in the FDM technique.

Ranganathan et al. [165] described the influence of glass fibres and glass beads on the thermal properties of composites made of polyamide 6 (PA6). Composite samples were obtained by the FDM method. The analyses show that the introduction of glass fibre into the polymer increases thermal conductivity and heat distortion temperature. For 30 wt.% of glass fibre, an increase in values of 140% and 130% was obtained, respectively, for heat distribution temperature and thermal conductivity in relation to neat polymer. Luke et al. investigated the effect of continuous glass fibre content and orientation on the mechanical properties of reinforced nylon. The materials tested in terms of mechanical properties contained 9.5%, 18.9%, 28.4% by volume of fibres with an orientation between

0° and 90° (with an increment of 15°). The tensile strength parameter increased with the fibre content in the polymer matrix. For the lowest fibre content (9.5% by volume), 122 MPa was obtained, while for the highest, i.e., 28% by volume, this parameter was 291 MPa. The change of the fibre angle from 0° (parallel to the tensile stress) to 15° lowered the tensile strength value for the 28% vol. fibres by 78% (from 291 MPa to 64 MPa), which indicates the significant influence of the fibre orientation in the polymer [166]. Dickson et al. also investigated the effect of GF on nylon properties (proprietary grade provided by the manufacturer). Mechanical strength tests show that the GF additive increased the tensile strength parameter by 91 MPa for GF-concentric and by 151 MPa for GF isotropic compared to neat Nylon, with a simultaneous decrease in elongation at break. The flexural strength values increased significantly by 123.81 and 154.77 MPa for GF-concentric and GF isotropic, respectively, compared to the reference. The authors of the study note that with the increase in the volume fraction of fibres, larger amounts of air are also introduced into the matrix, which affects the mechanical properties. The best results were obtained for materials with a filler content of up to 22.5%. Samples with fibre content up to 33 vol.% showed only a slight improvement in mechanical properties [167]. Chabaud et al. described the hydromechanical properties of GF/PA composites, which are to be a potential structural application. The authors of the work characterised the materials by sorption, hygro-expansion, and mechanical properties in a wide range of relative humidity (10–98%) [168].

There are also examples in the literature of reinforcing polylactide (PLA) with glass fibres. A recovery of glass fibres from wind turbines has been described, together with production of PLA/GF granulates using a twin-screw extruder, and then obtaining a composite filament on a single-screw extruder. The samples for analysis were prepared by the FFF method. The performed mechanical tests showed an 8% increase in Young's modulus compared to the reference sample of unmodified PLA; however, the authors did not report a significant improvement in tensile strength. The SEM images of the samples showed broken fibres, which is the result of the load transfer between the PLA matrix and GF [169]. Li et al. also described the effect of GF additive on PLA. It can be seen from the conducted analyses that the addition of 4 wt.% glass fibres improve the hardness, but on the other hand lowers the toughness. The addition of 8 wt.% of glass fibre significantly increased the brittleness of the material and its hardness [170]. The next work [171] describes not only the properties of the obtained PLA/continuous glass fibre composites, but also the innovative method of 3D printing. The first step involved preparing the filament with melt impregnation, and then printing the materials on a modified 3D printer. The process was optimised in terms of the amount of fibres in the matrix, the amount of compatibiliser (PLA grafted with maleic acid glycoside), and the printing parameters, i.e., nozzle diameter, edge width, layer thickness, printing speed, and temperature. Optimised parameters allowed composites with 45% GF content to be obtained. The addition of a compatibiliser increased the forces of interfacial interactions between the polymer matrix and glass fibres. The obtained materials (45 wt.% of GF) were characterised by high values of flexural strength and flexural modulus (respectively 313 MPa; 21.5 GPa). Another work shows that the addition of 4 vol.% of glass fibres to the PLA matrix increases the tensile strength parameter by 57% [172].

Another polymer known in the literature that has been reinforced with glass fibres is PEEK (heat-resistant polyetheretherketone). Reinforced composites with 5 wt.% of GF were obtained. The authors of the study also investigated the influence of the nozzle temperature, table temperature, printing speed, and layer thickness on the mechanical properties (tensile strength, flexural strength, and impact strength) of materials. The conducted tests showed an increase in the tensile and flexural strength parameters of glass fibre-reinforced composites due to the “pinning” effect of the fibres compared to neat PEEK. However, the impact strength of materials with the addition of GF is lower, which was explained by the authors on the basis of morphological changes (creating a porous structure) and degradation of the molecular chain [173].

5.3. Carbon Fibres

5.3.1. General Considerations

Carbon fibres (CFs) are fibres which contain 90–100 wt.% carbon atoms arranged in planar hexagonal networks [174]. They can be produced from different polymeric precursor materials, such as polyacrylonitrile (PAN), cellulose, pitch, and poly(vinyl chloride) [175]. PAN precursors account for 90% of the carbon fibre market [176]. Contemporary carbon fibre production from PAN requires solution spinning PAN into fibres, thermooxidatively stabilising the fibres in the air in the temperature range of 200–400 °C, and finally carbonising the spun fibres at high temperature in the range of 1000–1700 °C. Ultra-high-performance carbon fibres can be created by graphitising the fibres at temperatures ranging from 2500 °C to 3000 °C after carbonisation [174].

From a macro perspective, carbon fibres are very thin filaments (about 5–10 µm in diameter), which are just barely visible to the human eye. Due to their high elastic modulus (up to 940 GPa) and tensile strength (up to 5.7 GPa), as well as low density, these fibres, along with different polymer matrices, form composite materials called carbon fibre-reinforced polymer (CFRP) composites, that can be formed into rigid components with tailored directional properties for great weight savings compared to conventional engineering metals [174]. CFRP found applications in the automotive and aerospace industries, as well as wind turbines, etc. [177]. Therefore, filaments for 3D printing with CFs have become a subject of interest.

5.3.2. PLA-Based Composites

As mentioned above, CFs are used mainly for reinforcing and reducing the weight of the final product. For the same purpose, they are used also in 3D printing. One needs to keep in mind that there are a lot of factors affecting the final properties of 3D-printed models. El Magri et al. [178] observed the effect of printing properties on the mechanical properties of CF-reinforced PLA parts. Mechanical properties showed an improvement in Young's modulus and tensile strength as a function of nozzle temperature and reached their maximum at 230 °C. Maximum values of 2622 MPa and 3553 MPa for the Young's modulus were thus obtained, respectively, for PLA and PLA-CF. The addition of CFs increased crystallinity slightly, which was explained by the alignment of CFs in the direction of 3D printing as well as the orientation of polymeric chains toward CFs during the cooling process. However, increasing nozzle temperature led to a progressive decrease in the crystallinity level for PLA. For PLA-CF, the same tendency is observed in the 180–220 °C range. The optimisation of printing parameters on mechanical properties of CF-reinforced composites was done also for ABS [179] or other polymers and the effects of the fibre orientation, stacking sequence, matrix infill pattern, infill density, raster angle, layer thickness, build orientation, platform/printing temperature, deposition speed, or annealing temperature is summarised in [180].

Ansari and Kamil [181] used CFs for increasing impact strength and hardness of PLA, with the maximum hardness increasing up to 79.6 (Shore D), while the maximum impact strength was 114 J/m, which was 38% and 2.85× higher than the neat polymer, respectively. The addition of milled carbon fibres increased the thermal conductivity of PLA [182]. The enhanced thermal performance was useful in determining whether the 3D-printed parts had any porosity. Bakis et al. [183] described alignment in filament in the measured tensile moduli and strength of feedstock and unidirectionally printed material. From the results presented for stiffnesses, it can be concluded that the short CFs increased the tensile modulus E1 (relative to the printing direction) of the reinforced PLA/CF by about 2.2 times in comparison to the same property of the neat PLA. The tensile modulus E2 (transverse to the printing direction) and the shear modulus G12 (relative to the plane of printing) were also increased by the addition of the short fibres, 1.25 and 1.16 times, respectively, therefore not as much as E1 was. Moreover, the Poisson coefficients were provided to show the mechanical anisotropy of the prepared materials [184]. The mechanical properties can be improved by the annealing of the 3D-printed samples [185]

or the decreasing of layer thickness [186]. Al Zahmi et al. [187] used recycled PLA for low-cost applications. They found the recycled PLA showed a higher level of ductility by 15% when compared to the commercial PLA filament. For the CF/PLA, the CF has an opposite impact on the ductility: it decreased the strain at the failure by 43% and 30% for 10% and 20% CF, respectively.

5.3.3. ABS-Based Composites

ABS with 5% of CF exhibits a relatively high porosity (up to 19%) and prevents it from being mechanically and structurally stable comparable to neat ABS or ABS reinforced with CNTs [188]. Tekinalp et al. [189] compared 3D-printed and compression-moulded samples of ABS with chopped CF (up to 40%). The tensile strength and modulus of the 3D-printed samples increased by 115% and 700%, respectively. Indeed, 3D printing yielded samples with very high fibre orientation in the printing direction (up to 91.5%), whereas the compression moulding process yielded samples with significantly lower fibre orientation. Microstructure–mechanical property relationships revealed that although a relatively high porosity is observed in 3D-printed composites as compared to those produced by the conventional compression moulding technique, they both exhibited comparable tensile strength and modulus. This phenomenon is explained based on the changes in fibre orientation, dispersion and void formation. Ning et al. [190] compared different content and length of CFs in ABS plastic; adding CFs could increase tensile strength and Young's modulus, but may decrease toughness, yield strength, and ductility. The specimens with 150 μm carbon fibre had larger tensile strength and Young's modulus than those of 100 μm . Compared with the CFRP composite specimen with 100 μm carbon fibre, the 150 μm ones had smaller toughness and ductility. There was no significant difference in yield strength value between these two kinds of specimens. The addition of CFs to ABS increased the thermal conductivity, decreased the coefficient of thermal expansion (CTE), and greatly reduced the distortion of the parts [191,192].

5.3.4. Polyamide-Based Composites

de Toro et al. [193] compared PA6 composites filled with 20 wt.% of short CFs prepared by 3D printing and injection moulding (IM). Both the 3D printing and IM processes led to the breakage of fibres, making them shorter by up to 24%. Tensile tests of printed parts showed worse results than for the IM parts, but differences did not exceed 21% for either yield strength, tensile strength or Young's modulus. The compression tests revealed a more similar behaviour of 3D-printed parts and IM parts (only 4% improvement). Printed samples had higher stiffness values than the IM parts. The reinforcing effect was also confirmed for PA when 15% of short CFs had the highest values of both tensile, 90.8 MPa, and flexural strength, 114 MPa [194]. Furthermore, it was observed that the increase in the infill density determines the decrease in the glass transition temperature. The thermal conductivity of PA12 filled with CNTs grafted on chopped CFs was improved only slightly [195]. Comparing the fibre reinforcing, it was found that the nylon composite (based on the proprietary nylon grade provided by the manufacturer) strength was in the following order: carbon fibre > glass fibre > Kevlar fibre [167]. These results were also confirmed by the other authors [159,196,197].

5.3.5. PETG-Based Composites

Another studied polymer with CF used for 3D printing is PETG. Špitalský's group studied native polymer matrix and cheaper recycled matrix filled with CF up to 20 wt.% when they observed that replacing a virgin matrix with a recycled matrix does not significantly change the properties of the filament, and just causes a price reduction. The best sample had a 124% higher E than the neat polymer matrix. As the increase in CF content also increased the tensile stress at yield and rupture, the material became more resistant to permanent (plastic) deformation. A decrease in the ϵ_B of the prepared CF composites was observed. The same effect was observed for nanoindentation measurements. The E_r was in-

creased with the increasing loading of CF up to 150% compared to pure polymer matrix, but H remained constant at the same value of about 140 MPa [198]. With similar reinforcement of PETG, microscopic analysis revealed a 12% of void spots and fibre alignment according to the deposition path [199]. In another work [200], the experimental results revealed flexural stress of 66.9 MPa for neat PETG, and 79.2 MPa for the PETG/CF composite. These results were better for CF than for Kevlar fibres. Furthermore, it was shown that, compared to neat PETG, when carbon fibres were added, the thermal conductivity of the composite increased by around 5%. The opposite results were observed by Valdez where the decrease of compressive properties was measured [201]. This effect was also confirmed by cyclic compression [202].

5.3.6. PEEK-Based Composites

There are also other polymer matrices studied for 3D printing by the FFF/FDM method that use CFs. In the case of PEEK, the addition of short fibre led to the porosity increase of composites, and the ductility of the material is also reduced; the maximum tensile strength of 5 wt.% CF/PEEK in this experiment is 94 MPa, which is about 19% higher than that of 3D printing neat PEEK. Both tensile and flexural strength of CF/PEEK decreased monotonically with the increase of fibre weight percentage in the range of 5 to 15 wt.%. The thermal stability of composites was also improved compared with that without the addition of fibre [203]. Based on the impact properties of 3D-printed test samples from CF composites, HIPS material is considered semi-plastic and PC as plastic [204]. PC filament with short CFs has a decreasing effect on the ductility and toughness with an increasing concentration of CFs. Opposite to this, a significant increase in the strength and modulus is observed due to the strong adhesion between the fibre and matrix [205].

5.3.7. Continuous CF-Reinforced Systems

The independent group of CF-reinforced polymer composites for 3D printing is an area of continuous CF composites which has been developed during the last 10 years [206]. Because there are several differences in the feeding of filaments (towpreg extrusion, in situ impregnation and co-extrusion with towpreg) compared to “common” feeding in FFF 3D printing, we will not focus on this area. It is available for PLA [207], epoxy [208], PEEK [209], or PA [210]. More details can be found in several reviews dedicated to continuous CF-reinforced polymers manufactured by fused filament fabrication, e.g., [211]. One example is the comparison of CFs in nylon. The tensile strength and stiffness of the continuous fibre printed parts were 986 MPa and 64 GPa, respectively, which is more than an order of magnitude higher than the short fibre-reinforced Nylon printed parts (33 MPa and 1.9 GPa) [212].

5.4. Basalt Fibres

Sang et al. tested PLA-based systems with varying loading of APTES-modified basalt fibres (BFs) (5–20%) of different fibre lengths, and additional systems with carbon fibres (CFs) as the reinforcing phase. The FDM-fabricated samples were then compared to the ones prepared by compression moulding [213]. BF-reinforced composites showed much less severe rise in the melt viscosity than CF-reinforced ones, which translated to better printing feasibility and less microstructural defects in the produced specimens. In other work, they investigated PLA-based composites and composite blends with various amounts (17–34%) of polycaprolactone (PCL) and constant amount of 15% *w/w* APTES-modified BFs for 3D printing of honeycomb structures of different unit cell shapes for energy-absorbing applications [214]. The impact of polymer blending on the mechanical, thermal and thermomechanical properties of the composites and the effect of honeycomb unit cell on the mechanical performance of the systems were studied. The addition of PCL reduced the brittleness of PLA, improved the ductility and elasticity of the composite, and facilitated matrix–filler adhesion; the PCL-PLA/BF composite honeycombs showed elastic response to compression and superior energy absorption when compared to PLA/BF systems.

Yu et al. studied PLA-based composite containing 15 wt.% of BFs [215]. By means of 3D X-ray microscopy combined with computer tomography (CT) simulation analysis, they investigated the microstructure anisotropy of the 3D-printed composite. The work proved the orientation of the fibres are in accordance with the raster orientation during the printing process and that the shear stress generated in the nozzle enforces the uniform distribution of the fibres within the printed composite piece. The important conclusion was that changing the printing direction allows the tuning of the mechanical properties of the sample. In another work, they analysed the matrix–filler–void anisotropy effects of composites containing 5–20% of the filler [216]. The works discussed the inner- and inter-filament void formation mechanisms and modes, as well as their impact on the material rigidity, and emphasised the positive impact of the BF filler on the reduction of the inter-voids formation, while the inner-voids formation may be reduced by improving the matrix–filler interface.

Kurniawan et al. tested several methods for improving BF-PLA interaction [217]. As a control sample, commercially available, silane-treated basalt fibres were used. For BF modification, pyrolytic desizing at 450 °C, and subsequent treatment with either 3-glycidoxypyltrimethoxysilane or plasma-polymerised acrylic acid vapours was performed. For another approach, a compatibiliser was prepared in a form of maleic anhydride-grafted PLA (MAPLA), by reactive extrusion with utilisation of dicumyl peroxide as a free radical initiator. It was noted that desizing reduced the PLA-BF compatibility, while silanisation and plasma-assisted acrylic acid grafting significantly increased tensile strength of the composites. On the other hand, MAPLA addition resulted in decrease of composite storage modulus; however, due to the preliminary character of the presented study, the optimisation of MAPLA loading or maleic acid to PLA ratio during the grafting process was not explored.

Balaji et al. discussed the applications of basalt fibres in composites for the automotive industry, as well as examples of approaches towards their use in AM technologies, together with the strategies of surface modification of the filler towards the improved mechanical properties of the 3D-printed composites [218].

Zotti et al. tested PLA/BF composites containing 0–30% basalt fibres, KV-12 type, sized by the manufacturer with a proprietary silane agent. The fibres were used independently or together with 5–15% of either sepiolite or talc as a secondary filler [219].

Arslan et al. prepared ABS composites filled with 0–30 wt.% of APTES-treated BFs [220]. While BFs addition resulted in increasing the material's tensile strength by >20% and flexural strength by >60% for the highest filler loading, the composite suffered from reduced strain at rupture, as is common for filled plastics. BFs also slightly improved thermal stability measured by thermogravimetry, while decomposition T_{\max} was virtually unaffected, as well as T_g from DMTA.

Coughlin et al. prepared ABS composites containing 0–60 wt.% of BF [221]. Due to high filler loading, 60%-filled composite was found not suitable for FDM application, both the filament being found to be brittle to spool and feed, and the FDM process failing due to nozzle clogging, feeding issues, and printed part warping.

Dowling et al. investigated the effect of air atmospheric plasma treatment of continuous basalt fibre (CBF) surface for the 3D printing of reinforced polypropylene (PP) [222]. The filler was sized with a proprietary silane coupling agent by the manufacturer, the sizing agent claimed to be chosen for improved compatibility with PP. The plasma treatment provided increased modulus and strength (by means of flexural and short beam shear testing) of the composite. The effect was explained on the basis of enhanced interfacial bond strength, supported by computer tomography and optical microscopy. As the plasma treatment was performed at high feeding speed of CBF and in-line during filament extrusion, it is possible that PP grafting was occurring at the plasma-activated surface.

5.5. Nanosilica (*Aerosil*, etc.)

Nanometric silica is used as a filler for composite materials, mainly due to the improvement of their mechanical properties and very high thermal resistance. Its biggest disadvantages include the possibility of the formation of agglomerates caused by the interaction of the surface hydroxyl groups and the weak interaction of the polar surface of the filler itself with the matrix. The simplest method of preventing this phenomenon is the modification of silica with adhesion promoters, which results in better dispersion of the filler and influences its higher chemical affinity to the polymer matrix [223,224].

In the work of Wu et al. [225], nanosilica was modified with APTES and then incorporated into the PLA matrix; it was shown that the best results of filler dispersion are obtained for its low content of up to 1%. The influence of the chemical treatment on the improvement of the mechanical properties of the composites was found, in this case also the best results were observed at low loading of nanosilica; additionally, modified SiO₂ improved the thermal stability of the systems.

Gong et al. modified nanosilica using bis-(3-triethoxysilylpropyl)tetrasulfide (TESPT) as a silanising agent in order to improve the dispersion of nanoparticles in the matrix, and then such modified filler was added to PLA/natural rubber thermoplastic vulcanizate (TPV). In addition to improving dispersion, the reduction in surface tension also made it possible to improve the compatibility between the two phases. The modification improved the impact strength and mechanical properties [226]. The same authors investigated the effect of 3-methacryloxypropyltrimethoxysilane (MATMOS)-modified nanosilica in the same type of polymer matrix, and once again the improvement of modifier compatibility in the matrix and over 38-fold improvement in impact strength compared to neat PLA were observed [227].

Kodali et al. [228] tested polycarbonate aerosil composites with 0.5, 1 and 3 wt.% filler loading. The research showed an increase in thermal stability and tensile strength—the best effects were observed for the lower loadings. This effect can be explained by the fact that nanosilica improves the mechanical properties only in a certain favourable content, and exceeding it causes an increase in the brittleness of the material due to discontinuities within polymer volume and, as a result, the observed decrease in the tested parameters.

In subsequent published studies [229], PLA/nanosilica filament with a grain size of 20 nm was produced. Systems with a 2, 4, 6 and 8 wt.% filler loading were prepared. In this work, the highest increase in tensile and flexural strength, compression, and hardness at 8% filling was observed, additionally, a reduction in the coefficient of friction was observed.

Sharma and Singholi investigated the mechanical properties of MATMOS-modified nanosilica (50 nm average grain size) in 0–6 wt.% loading for PLA/wood composite. Improvements in mechanical properties, such as an increase in flexural strength, compression strength, as well as increase in hardness, were observed. The most favourable results were achieved with the addition of 2% silica and were, respectively, 16.6%, 60% and 60%. An increase in thermal stability was also observed for all tested samples [230]. In other work, the same authors investigated the effect of MATMOS-modified nanosilica and nanoalumina on the properties of PLA/wood composite. Filaments containing 2% of each filler and a mixture of 2% nanosilica + 2% nanoalumina were produced. Addition of fillers improved the hardness, compressive strength, and flexural strength, as well as thermal stability [231].

One of the biggest disadvantages of PLA is its high hygroscopicity. The research carried out in the paper [232] involved the use of proprietary silanol-treated nanosilica at 1 and 3 wt.%, unmodified silica was used as a reference system. The modifications carried out showed a reduced moisture absorption by the composite. Better results were obtained for 1% loading. Higher tensile strength and Young's modulus was also obtained for each modification.

Vidakis et al. investigated the influence of nanosilica on the properties of the isotactic PP homopolymer. The addition of the filler improved the mechanical properties for both 1, 2 and 4% loading, and rheological tests showed that the addition of silica did not deteriorate the processability of the composite [233]. The authors also conducted research

on the preparation of SiO₂/PLA composites and observed the influence of the filler on the mechanical properties, the highest increase was observed for a composite containing 1% of filler, and a decrease in mechanical strength was observed with the increase in its content. In the study, antibacterial measurements were carried out, and mild antibacterial properties against *S. aureus* were observed for composites with 4% loading [234].

5.6. Carbon Materials-Graphene, Graphite, Soot

Carbon forms many allotropes. Its structure determines its properties. A three-dimensional allotrope of carbon-graphite, is known from ancient times and consists of individual layers of another one-dimensional carbon allotrope-graphene [235], while zero-dimensional fullerenes (carbon molecules that are characterised by a symmetrical closed-cage structure) and one-dimensional nanotubes (CNTs) were discovered in the last century. Another known carbon structure for polymer composites is known as carbon black (CB)-grape-like aggregates of highly fused spherical particles [236]. Members of the carbon particle family have shown unique features and have been widely exploited in biomedicine, agriculture, food industry, electronics, plastic industry, energy industry, etc. [237]. The carbon-filled composites with high electronic conductivity are attractive in many potential applications, especially in the field of electronics, including energy storage devices, sensors, and electrically conductive structures. Compared to electronics and electrochemical devices manufactured by conventional manufacturing techniques, such as slurry casting and coating nanomaterials on the substrate, 3D printing provides a simplistic, rapid, and low-cost approach to producing these electronics with complex structures. In addition, 3D printing allows manipulating the structure of the components by overcoming the limitations of electronics and electrochemical devices (i.e., the trade-off between the power and energy of conventional electrodes, a lack of scalability and the high cost of producing high-resolution sensors). As 3D printing for these products has been actively studied, they exhibit better performance in terms of high areal energy and power density, and high sensitivity, compared to the conventional electrodes and sensors, respectively [238].

Biodegradable PLA may be used in combination with conductive carbon filler for different 3D applications. In the work of Foster [239], PLA filament loaded with ≈ 8 wt.% graphene was prepared for the 3D printing of disc electrodes for energy storage devices. The addition of graphene enhanced the thermal properties of the filament. It was applied as freestanding lithium-ion anodes and solid-state graphene supercapacitors. Additionally, this 3D electrode (3DE) platform has been analysed for its ability to create hydrogen via the hydrogen evolution reaction, in which these 3DEs exceed expectations and exhibit an extremely competitive onset potential compared to that of a platinum electrode. The addition of graphene also improved nanohardness by 18%, increased the elastic modulus of PLA/graphene by 11% and resistance to displacement (25%), suggesting there is a higher resistance to plastic deformation in the reinforced samples. This behaviour can be attributed to the effective transfer of stress to graphene reinforcement. During the unloading period, PLA/graphene can recover 43% of the elastic deformation experienced, while PLA was able to recover 25%, indicating that the presence of graphene in the filament decreases the permanent deformation. Wear resistance was increased by 14% in PLA/graphene as compared to the neat PLA [240]. In the other work, it was observed that PLA/graphene nanoplatelets (GNP) composite samples showed the best performance in terms of tensile and flexural stress (about 1.7 times higher than PLA). In addition, PLA/graphene composite samples showed the highest interlaminar shear strength (about 1.2 times higher than neat PLA samples). However, the addition of GNPs tended to reduce the impact strength of the PLA/graphene composite samples (PLA samples exhibited an impact strength about 1.3 times higher than PLA/graphene composites). Furthermore, the addition of graphene nanoplatelets did not affect, in general terms, the dimensional accuracy of the PLA/graphene composite specimens. In addition, PLA/graphene composite samples showed the best performance in terms of surface texture, particularly when parts were

printed in flat and on-edge orientations [241]. The addition of carbon materials enhances the thermal conductivity of the material, and this fact is used also for welding of 3D-printed samples. The addition of CNTs and microwave irradiation was shown to improve the weld fracture strength by 275% [242]. The Ivanov group observed a small synergistic effect in the GNP/MWCNT/PLA bi-filler hybrid composites when combining GNPs and CNTs at a ratio of 3% GNP: 3% CNT and 1.5% GNP: 4.5% CNT, showing higher electrical conductivity in comparison to the systems incorporating individual CNTs and GNPs at the same overall filler concentration. This improvement was attributed to the interaction between CNTs and GNPs, limiting GNP aggregation and bridging adjacent graphene platelets, thus forming a more efficient network (percolation effect). The thermal conductivity increases with higher filler content; this effect was more pronounced for the mono-filler composites based on PLA and GNP due to the ability of graphene to better transfer the heat [243]. In the work of Foo et al. [244], another 3D-printed electrode from PLA/graphene composite was prepared using a commercial 3D printer. The as-fabricated supercapacitor provided a good capacitance performance, with a specific capacitance of $98.37 \text{ F}\cdot\text{g}^{-1}$. They had a photocurrent response that exceeded expectations ($\approx 724.1 \mu\text{A}$) and a lower detection limit ($0.05 \mu\text{M}$) than an ITO/FTO glass electrode. In another work, a graphene/PLA filament was used to print a disc electrode, which demonstrated an unexpectedly high catalytic activity towards the hydrogen evolution reaction (-0.46 V vs. SCE) upon the 1000th cycle, such potential being the closest observed to the desired value of platinum at (-0.25 V vs. SCE) [239]. Chen et al. [245] prepared filaments blending TPU with PLA (with TPU to PLA ratio fixed at 7:3.) with the addition of graphene oxide (GO). They observed compression modulus constantly increasing with the loading of GO up to 167% for 5 wt.% GO. Tensile modulus and yield point have increased by 75.50% and 69.17%, respectively, at 0.5 wt.% loading of GO, which indicates that the addition of GO has significantly improved the tensile strength of the materials. However, when GO loading was further increased, both the tensile modulus and yield point decreased. The TGA and DSC data both demonstrated that the thermal stability of the TPU/PLA blend has been significantly improved by the addition of GO, with a 90°C increase in degradation temperature as well as the formation of better crystalline structures. Cell culturing results revealed the excellent cell viability of 3D-printed scaffolds, indicating that addition of limited amounts of GO has no obvious toxicity to cell growth, and a small amount of GO is beneficial for cell proliferation.

TPU filaments can be used for 3D printing of the multiaxial force sensors. The sensor had two components—a structural and a sensing part—both of which were fabricated by 3D printing with different functional material filaments. The structural part was printed with the commercial TPU filament and the sensing part was printed with CNT/TPU nanocomposite filament with a piezoresistivity on the surface of the structural part and an average resistivity of $0.143 \Omega\cdot\text{m}$ [246]. With the increased addition of MWCNTs, the material strength, initial elastic modulus, and electrical conductivity all increased. The increased modulus in the presence of MWCNTs greatly enhanced the printing capability of soft TPU by increasing the resistance to buckling. Very modest decreases were observed in the elasticity modulus, only $\approx 14.4\%$. This indicated an excellent adhesion between the TPU layers during the fusion process. As a result of such adhesion, no degradation was observed in the electrical conductivity, in both through-layer and cross-layer directions, of the nanocomposites after printing. The piezoresistivity gauge factors for the FDM 3D-printed and bulk samples were found to be similar, indicating that the printed samples performed with no decay under applied strains as large as 100%. It was shown that different MWCNT contents can provide different ranges of flexibility and sensitivity, tunable for particular applications [247]. Xiang et al. 3D-printed 1.5 wt.% TPU/CNT nanocomposites exhibiting higher tensile modulus (20.3 MPa) and strength (16.5 MPa) and comparative elongation (710%) relative to the printed neat TPU sample. Compared with the printed 3 wt.% TPU/CNT nanocomposite, the resistivity of TPU/CNT composite containing CNTs surface-modified with 1-pyrenecarboxylic acid (PCA) decreased by 37 times in the cross-layer direction at the same CNT loading. Highly flexible strain sensors exhibited

high sensitivity ($GF = 117$ and 213 at a strain of 250% for the printed sensor of 1.5 wt.% CNT/TPU) and a large detectable strain. Furthermore, the sensor performed well in the frequency range of 0.01 – 1 Hz and showed the capability to monitor the strains with different frequencies. In addition, this sensor showed excellent stability during cyclic strain testing up to 1000 cycles [248].

In the case of ABS, it was demonstrated that CNT content has a significant influence on the mechanical properties and electrical conductivity of 3D-printed samples. Printed samples obtained from high CNT content composites exhibited an improvement in the tensile strength of 12.6% and resistivity of $0.15 \Omega \cdot m$ for 9.09 wt.% loading of CNTs [249]. In the work of Sezer [250], the tensile strength increased by 206% for 10% MWCNTs loading as compared to the neat polymer. There was almost a linear increase for 3 , 5 , 7 and 10% MWCNTs loading with a maximum achieved at 10% (668% increase over neat ABS). The highest electrical conductivity value achieved for the 10% MWCNTs loading was $232 \times 10^{-2} S/cm$. MFI values dramatically decreased with MWCNT loading, reaching 0.03 g/10 mm value for 10% loading, explaining the nozzle clogging problem during the 3D printing process using filaments with higher MWCNT filler rates. Thermal properties of neat ABS were significantly influenced by the addition of CNTs. While a decrease of specific heat c_p (-11%) was observed, thermal diffusivity α ($+55\%$) and conductivity λ ($+30\%$) increased with a CNTs amount of 6 wt.% for bulk materials at $25^\circ C$ [251]. The SWCNT-filled (5 wt.%) composite demonstrated improvements of 31 and 93% in tensile strength and modulus, respectively. The SWCNTs provided more reinforcement than the CFs, and alignment was beneficial to the strength and modulus [252]. Another filament with graphene prepared by in-situ reduction of GO in ABS by hydrazine reached the value of conductivity $6.4 \times 10^{-5} S \cdot m^{-1}$ (at 3.8 wt.% loading of graphene). After it was 3D-printed into a 10 mm \times 10 mm \times 1 mm rectangular model, its measured conductivity decreased to $2.5 \times 10^{-7} S \cdot m^{-1}$. In FDM, the internal voids among adjacent stacked filaments may account for the falloff in conductivity. The highest graphene-loaded printable composite (5.6 wt.%) bears a conductivity of $1.05 \times 10^{-3} S \cdot m^{-1}$. The storage modulus results showed that G/ABS composites are higher than neat ABS polymer in the glass transition regime between $102^\circ C$ and $113^\circ C$. The DMA results of G/ABS composites demonstrated a more elastic behaviour as compared with neat ABS, suggesting enhanced stiffness of the material. All samples including ABS and its graphene composites exhibited less than 1% expansion under heating from RT to T_g [253]. Upon addition of 4 wt.% of GNP, the elastic modulus increased by about 30% compared to unfilled ABS. Due to the orientation of polymer during extrusion, in the entire temperature range, the storage modulus of extrudate is higher than that of compression-moulded samples and FDM-printed parts. Due to the GNP addition in the ABS matrix, the storage modulus of CM, extrudate and FDM parts increases by about 30 – 50% with respect to the neat ABS below the T_g . The effect of GNP nanofiller is manifestly more evident above T_g . In fact, the storage modulus of composite materials at $125^\circ C$ is more than twice that of neat ABS for all the investigated samples. The coefficient of linear expansion (CLTE) values of neat ABS up to $50^\circ C$ are in the range of 60 – $75 \times 10^{-6}/K$. After the addition of graphene nanoplatelets, CLTE was remarkably reduced with values in the range 44 – $66 \times 10^{-6}/K$, which means better dimensional thermal stability of the material in all the temperature intervals [254]. In the case of graphite application in ABS composites production, due to the layered structure of the filler, the reinforcement of the mechanical properties for recycled ABS with graphite is not so significant [255]. In the work of Aumnate et al., ABS/GO (graphene oxide) composite filaments were produced using dry mixing and solvent mixing methods before further melt being extruded, to investigate the proper way of dispersing GO within the ABS matrix. From the typical stress-strain tensile curves and corresponding statistical data, the elongation at break value decreased with the GO loading. The elongation at break value of neat ABS was determined as 5.8% , while the value for ABS/GO composite was 2.9% . However, by adding 2 wt.% of GO, the tensile strength and Young's modulus of ABS were enhanced [256]. For ABS with 15 wt.% of carbon black (CB), it can be concluded that the resistivity of

the printed samples increased remarkably. Specifically, the resistivity increased from $29.06 \Omega \cdot \text{m} \pm 0.77 \Omega \cdot \text{m}$ for the filaments to $42.59 \pm 1.94 \Omega \cdot \text{m}$ and $101.60 \pm 6.85 \Omega \cdot \text{m}$ for the cubic samples in the horizontal direction and the vertical direction, respectively [257].

The addition of CNTs showed a shift of the melting and crystallisation peaks towards higher temperatures compared to plain PEEK but had almost no effect on tensile properties [258]. PEEK/MWCNT (multi-walled carbon nanotubes) nanocomposites revealed an electrical percolation threshold taking place between 2 and 3 wt.% loading of CNTs. The incorporation of GNPs induced a further increase in the electrical conductivity levels attained, albeit moderate. Combinations of 3 wt.% CNT with higher loadings of GNPs, or of 4 wt.% CNTs with lower loadings of GNPs, showed consistent electrical conductivities of approximately 10 S/m. Interestingly, the incorporation of GNPs into the matrix had a less adverse effect on the processability than that of MWCNTs. The addition of MWCNTs/GNPs to PEEK reasonably improved Young's modulus and the yield strength, while reducing the ductility of PEEK filaments. The thermal conductivity was also enhanced. The 3D-printed tensile bars showed an improved modulus and a higher ultimate tensile strength, but a much smaller elongation at break as compared to the extruded filaments. A loss of electrical conductivity of two orders of magnitude was observed from filament to raft and to 3D-printed part [259].

Zhu et al. [260] compared samples prepared by 3D printing and compression moulding of PA12 with graphene nanoplatelets. The GNPs were overall uniformly dispersed in the PA12 matrix at lower contents (2, 4 and 6 wt.%), while GNPs agglomerates could not be avoided even at the lowest level of content due to the large size of utilised GNPs which were difficult to disperse. The optimal GNPs content of 6 wt.% was determined by the slightly decreased crystallinity which implied higher printing accuracy, but also higher thermal stability, improved thermal conductivity (+51.4%), and improved elastic modulus (+7%), along with an appropriate MFI value, than that of compression-moulded parts. In another work, multiscale thermoplastic composites consisting of proprietary polyamide copolymer (Pac), copoly(ester amide) (Vectra B950) copolymer reinforced with thermotropic liquid crystalline polymer (TLCP), and carbon nanotubes (CNTs) were generated. The copolymer was reported to be a random copolymer resulting from a reaction of 60 mol.% 2-hydroxy-6-naphthoic acid, 20 mol.% terephthalic acid, and 20 mol.% aminophenol. The most improvement in tensile properties due to the 1 wt.% addition of CNTs was observed to be for the 20 wt.% TLCP/1 wt.% CNTs/Pac samples. The resulting composite filaments exhibited 225% and 80% improvement in the tensile modulus and strength, respectively, compared to the composites without CNTs. In addition, 40 wt.% TLCP/1 wt.% CNT/Pac 3D-printed specimens with filaments laid parallel to the printing direction exhibited excellent tensile modulus and strength of 38.92 GPa and 127.16 MPa, respectively. The measured tensile modulus of 40 wt.% TLCP-reinforced composite is even higher than the reported 69 wt.% long glass fibre or 26 wt.% long carbon fibre-reinforced nylon in fused filament fabrication with the same printing pattern [261]. In the work of Zhang et al. [195] CNTs and GNPs/CNTs were used to modify PA12 to improve its thermal conductivity. Moreover, 7 wt.% CNTs improved the thermal conductivity (0.44 W/mK v.s. 0.28 W/mK for neat PA12) and electrical conductivity of the PA12, but the filler agglomeration was observed. PA12 with 15 wt.% of GNPs and 1 wt.% CNTs demonstrated the most improved thermal conductivity (0.73 W/mK), and a processability assessment for FFF 3D printing technology was conducted to determine the processing window for the selected composition.

Gnanasekaran et al. suggested that at least ≈ 0.49 wt.% of CNTs (≈ 0.31 vol.%) and ≈ 5.2 wt.% of graphene ($\phi_c \approx 3.3$ vol.%) are required for the fabrication of PBT-based conductive filaments for the FDM method [262]. The addition of conductive fillers improved the thermal stability, as both the onset and the maximum degradation temperature shifted to higher values. The presence of the conductive fillers facilitated heat conduction and acted as a barrier to inhibit the emission of decomposition products during combustion. The PBT/CNT composite exhibited higher thermo-oxidative stability than the PBT/G composite. The stiffness of the PBT/CNT 3D-printed monolayer was significantly higher

than that of the PBT/G composite; more precisely, the storage modulus was 28% higher for the PBT/CNT at 25 °C. In the work of Spitalsky [198] PETG filaments were filled with expanded graphite (EG) up to 10 wt.% and compared native and recycled polymer matrices. With increasing content of EG, the E increased, so that the material became stiffer. Tensile stress at yield (σ_Y) and tensile stress at break (σ_B) did not change significantly with the addition of EG, but for the highest concentration of filler (10 wt.%) they dropped sharply. The same effect was confirmed from nanoindentation measurements. EG had a synergic effect on mechanical properties with CF, however. The value for the thermal expansion coefficient slightly decreased from the value for virgin PETG, $\approx 60 \times 10^{-6} \text{ K}^{-1}$ up to $\approx 51 \times 10^{-6} \text{ K}^{-1}$. The wettability analysis showed that the addition of EG to PETG resulted in reduced contact angle values.

Kwok et al. prepared conductive filaments dedicated for 3D printing of electrical circuits and sensors, that were made from PP and CB [263]. The results suggested a percolation threshold below 11.3 wt.% (5.2% by volume). The effect of UV irradiation on the electrical resistance of the printed plastic wires was observed with no statistically significant difference before and after the UV stress test. The conductive thermoplastic composites remained stable for use at 12 V AC for at least one week without a drift in their electrical resistance. Between 60 V and 120 V, resistive heating melted and distorted the shape of the tested filaments and greatly increased the resistance of the printed arrays after stress. Thus, such prepared conductive filaments are unsuitable for applications that require a relatively high voltage (>60 V, AC) supply, and significant current. All the printed conductive filaments tested here displayed Positive Temperature Coefficient (PTC) effect, in which an increase in temperature led to an increase in electrical resistance. Han et al. prepared the filament of PP with an addition of maleic anhydride-grafted polypropylene (MAPP, 16 wt.%), thermotropic liquid crystalline polymer (TLCP) and CNTs [264]. That PP material exhibited a 265% improvement in the tensile modulus of the filaments. The tensile modulus of the filament with 1 wt.% CNT-reinforced composite was competitive with 9 wt.% continuous carbon fibre-reinforced nylon composite materials in FFF. Barrett's group prepared 3D-printed sensing strips, with MWCNTs loadings up to 15% mass, whose function was reversible vapour sensors with the strongest responses arising with organic compounds capable of readily intercalating, and subsequently swelling the PVDF matrix (acetone and ethyl acetate). A direct correlation between MWCNTs concentration and resistance change was also observed, with larger responses (up to 161% after 3 min) generated with decreased MWCNT loadings. 3D-printed material had excellent conductivity of $\approx 3 \times 10^{-2} \text{ S/cm}$. Samples composed of three layers were also moderately more conductive ($159 \pm 4.8 \Omega$) than their single-layer counterparts (95Ω) due to an increase in cross-sectional area [265]. PVA with graphene was used for printing parts with enhanced electromagnetic interference (EMI) shielding capability via FDM. The EMI shielding efficiency (SE) of the printed PVA/GNP parts with a thickness of 2.43 mm reached 26–32 dB in the frequency range of 8–12.4 GHz, which can completely satisfy the requirements for practical applications. The addition of 8 wt.% graphene to PVA increased the water contact angle from 31.4° to 50.9° and the mechanical properties, yielding a Young's modulus of 49.1 MPa, the ultimate tensile stress of 10.6 MPa, and elongation at break of 128.4% [266]. EVA tensile sensor from filament filled with graphite up to 50 wt.% had maximum electrical conductivity $2.3 \times 10^{-4} \text{ S cm}^{-1}$, which was 539 times higher compared to EVA, but resulted in the decrease in tensile properties and increasing compression properties of 172% [267].

5.7. Other Fillers

Castles et al. presented the production of a series of composites containing different contents of BaTiO₃ microparticles in an ABS matrix, which can be used for 3D printing. Microwave dielectric properties of printed materials with a content of 70 wt.% BaTiO₃ has been characterised using a 15 GHz split post dielectric resonator (SPDR). The materials exhibited relative permittivities in the range of 2.6–8.7 and Loss tangents in the range

of 0.005–0.027 [268]. Another work on BaTiO₃ in the ABS matrix presents the process of producing composites, as well as their mechanical and dielectric characteristics [269]. Nanocomposites were produced with a filler content of up to 35 vol.% BaTiO₃ (74.2 wt.%). Due to the brittleness of the material, composites with a 40 vol.% were not printable. With a content of 45 and 50 vol.% the composites showed stick-slip behaviour and could not be extruded in a reproducible manner. The mechanical characteristics showed that the brittleness of the material increased with the increase of the filler content. Composites with 35% by volume of BaTiO₃ were characterised by the tensile strength parameter of 13.7 MPa, while the value for neat ABS was 25.5 MPa. Similar results were obtained for the flexural strength tests. For samples of ABS containing 35 vol.% of the filler an increase in relative electric permeability to 11.5 at 200 kHz was observed, which was an increase of 8.42 compared to pure polymer.

Another method is to use BaTiO₃ nanowires in the PLA matrix, which are piezoelectric nanocomposites [270]. The conducted electromechanical studies show that proper alignment of nanowires significantly affects the efficiency of energy collection. Optimum power output can be increased up to 8 times for composites. Kim et al. prepared and characterised the BaTiO₃/PVDF nanocomposite produced by the FDM method. BaTiO₃ agglomeration effect in the polyvinylidene fluoride matrix was explained on the basis of the higher density of the filler compared to the matrix. The use of the FDM process allows for better dispersion and homogeneity. The BaTiO₃/PVDF composite 3D-printed with FDM exhibited a piezoelectric response three times higher than the solvent-casted nanocomposites [271]. Another work by the same team also presents 3D printing of BaTiO₃ in a poly(vinylidene) fluoride matrix as piezoelectric sensors [272]. The work by Paspali et al. presents the influence of the nanostructure on the mechanical properties of the printed polylactide/nanoclay composites by the FFF method. Commercially available sodium bentonite clays are modified with bis(hydrogenated tallow alkyl) dimethyl ammonium salt. The conducted mechanical tests show that the addition of 5 wt.% modified clay to PLA increased the tensile modulus by 10%, while reducing the tensile strength value by 15% [273]. C.H. Lee et al. investigated the effect of the powder dosing rate on the mechanical properties of the ABS-CuFe₂O₄ composite. The amount of filler was controlled by the speed of the powder dispenser. The conducted mechanical tests show that the addition of the filler at high speed to the ABS matrix reduces the strength from 17.1 MPa to 14.6 MPa, which is related to the agglomeration of the filler, as well as the creation of voids in the tested materials [274].

6. Conclusions

Within the last couple of years, a significant growth of interest in FDM printing composites with fillers of both natural and synthetic origin has been observed. Based on the characteristics of the fillers selected, printable systems of a number of new features may be obtained, from increased mechanical and thermal properties, to photocatalytic reactors, to biomedical or microelectronic and electromagnetic devices. Although the development of these novel materials is the testament to the Additive Technologies being one of the pillars of the Fourth Industrial Revolution, it is still a matter of heavy experimentation and optimisation until a large fraction of the assumed applications will be refined to the form of sophisticated solutions ready for the world market. Nonetheless, since the first development of the FDM technology in 1989, it has become a platform for fabricating special purpose-oriented materials, the number of applications of which being seemingly unlimited. The discussed review presented that a direct transfer from conventional processing technologies (extrusion, injection moulding) to FDM (which can be perceived as a microextrusion technology) does not always provide similar or expected results. Therefore, it is fully justified to perform independent material studies solely dedicated to the FDM composite area.

Author Contributions: Conceptualisation, R.E.P. and B.S.; methodology, R.E.P.; validation, B.S. and R.E.P.; formal analysis, B.S., R.E.P. and D.B.; resources, B.S.; data curation, M.F. and D.P.; writing—

original draft preparation, R.E.P., B.S., D.B., M.F., D.P. and Z.Š.; writing—review and editing, R.E.P.; visualisation, D.B., M.F. and D.P.; supervision, R.E.P. and B.S.; project administration, B.S.; funding acquisition, B.S. All authors have read and agreed to the published version of the manuscript.

Funding: This research was funded by National Centre for Research and Development, Poland, under the LIDER X project (LIDER/01/0001/L-10/18/NCBR/2019).

Data Availability Statement: The data used for the study was provided from Scopus database analysis.

Acknowledgments: Scientific research in the field of designing organosilicon modifiers of thermo-plastic properties for the incremental FDM technique financed from the sources of the National Centre for Research and Development under the LIDER X project (LIDER/01/0001/L-10/18/NCBR/2019). Z.Š. would like to thank the Slovak Grant Agency for financial assistance, project VEGA 2/0051/20.

Conflicts of Interest: The authors declare no conflict of interest.

Abbreviations

ABS	Acrylonitrile–butadiene–styrene terpolymer
AM	Additive Manufacturing
APTES	3-aminopropyltriethoxysilane
AR	Aspect ratio
BF	Basalt fibres
CAGR	Cumulative annual growth rate
CB	Carbon black
cFF	Continuous flax fibres
CLTE	Coefficient of thermal expansion
CNFRB	Continuous natural fibre-reinforced biocomposites
CNT	Carbon nanotubes
COP	Cyclo-olefin polymer
CPC	Cork polymer composites
DMA	Dynamic Mechanical Analysis
DMTA	Dynamic Mechanical Thermal Analysis
DSC	Differential Scanning Calorimetry
EDX	Energy-dispersive X-ray spectroscopy
EMI	Electromagnetic interference
EPDM-g-MAH	Ethylene-propylene-diene monomers polymer grafted with maleic anhydride
EVA	Ethylene-vinyl acetate copolymer
FDM	Fused Deposition Modelling
FF	Flax fibres
FFF	Fused Filament Fabrication
FRP	Fibre-reinforced plastic
FT-IR	Fourier-Transform Infrared
FTO	Fluorine-doped tin oxide
GF	Glass fibres
GNP	Graphene nanoplatelet
GO	Graphene oxide
HA	Hydroxyapatite
HBC	Hygromorph biocomposite
HDPE	High-density polyethylene
HDPE-g-MA	High-density polyethylene grafted with maleic anhydride
ITO	Indium-doped tin oxide
LDPE	Low-density polyethylene
LLDPE	Linear low density polyethylene
MAPLA	Maleic anhydride-grafted PLA
MAPP	Maleic acid-grafted polypropylene
MATMOS	3-methacryloxypropyltrimethoxysilane
MFI	Melt-flow index

MWCNT	Multi-wall carbon nanotubes
NFRP	Natural fibre-reinforced plastics
PA12	Polyamide 12
PA6	Polyamide 6
Pac	Polyamide copolymer
PAH	Polycyclic aromatic hydrocarbon
PAN	Polyacrylonitrile
PBAT	Poly(butylene adipate terephthalate)
PBS	Poly(butylene succinate)
PBSA	Poly(butylene succinate adipate)
PBT	Poly(butylene terephthalate)
PC	Polycarbonate
PCL	Polycaprolactone
PEEK	Polyetheretherketone
PEG	Poly(ethylene glycol)
PEI	Polyethyleneimine
PET	Poly(ethylene terephthalate)
PETG	Poly(ethylene terephthalate) modified with cyclohexyl-1,4-dimethanol
PLA	Poly(lactic acid)
PLGA	Poly(lactic-co-glycolic acid)
PMMA	Poly(methyl methacrylate)
POE-g-MA	Polyolefin grafted with maleic anhydride
PP	Polypropylene
PDLGA	poly(D,L-lactic-co-glycolic acid)
PTC	Positive temperature coefficient
PVA	Poly(vinyl alcohol)
PVDF	Poly(vinylidene difluoride)
PVPA	Poly(vinylphosphonic acid)
rABS	Recycled ABS
rPP	Recycled polypropylene
rPS	Recycled polystyrene
RT	Room temperature
SCP	Saturated calomel electrode
SEM	Scanning Electron Microscopy
SPDR	Split post dielectric resonator
SWCNT	Single-wall carbon nanotubes
T _g	Glass transition temperature
TG	Thermogravimetry
TLCP	Thermoplastic liquid crystalline polymer
T _{max}	Temperature of maximal rate of mass loss from TG
TPU	Thermoplastic polyurethane
TPU	Thermoplastic polyurethane
XRD	X-ray Diffractometry

References

1. Hull, C. Apparatus for Production of Three-Dimensional Object by Stereolithography. U.S. Patent 4,575,330, 11 March 1986.
2. Nguyen, N.A.; Bowland, C.C.; Naskar, A.K. A general method to improve 3D-printability and inter-layer adhesion in lignin-based composites. *Appl. Mater. Today* **2018**, *12*, 138–152. [[CrossRef](#)]
3. Vaidya, A.A.; Collet, C.; Gaugler, M.; Lloyd-Jones, G. Integrating softwood biorefinery lignin into polyhydroxybutyrate composites and application in 3D printing. *Mater. Today Commun.* **2019**, *19*, 286–296. [[CrossRef](#)]
4. Mazzanti, V.; Malagutti, L.; Mollica, F. FDM 3D printing of polymers containing natural fillers: A review of their mechanical properties. *Polymers* **2019**, *11*, 1094. [[CrossRef](#)]
5. Grand View Research, 3D Printing Market Size, Share & Trends Analysis Report by Component (Hardware, Software, Services), by Printer Type, by Technology, by Software, by Application, by Vertical, by Region, and Segment Forecasts, 2022–2030; Research and Markets: Dublin, Ireland, 7 July 2022.

6. Murphy, S.V.; Atala, A. 3D bioprinting of tissues and organs. *Nat. Biotechnol.* **2014**, *32*, 773–785. [\[CrossRef\]](#)
7. Tan, D.K.; Maniruzzaman, M.; Nokhodchi, A. Advanced pharmaceutical applications of hot-melt extrusion coupled with fused deposition modelling (FDM) 3D printing for personalised drug delivery. *Pharmaceutics* **2018**, *10*, 203. [\[CrossRef\]](#)
8. Najmon, J.C.; Raeisi, S.; Tovar, A. Review of additive manufacturing technologies and applications in the aerospace industry. In *Additive Manufacturing for the Aerospace Industry*; Elsevier: Amsterdam, The Netherlands, 2019; pp. 7–31.
9. Yadav, D.K.; Srivastava, R.; Dev, S. Design fabrication of ABS part by FDM for automobile application. *Mater. Today Proc.* **2020**, *26*, 2089–2093. [\[CrossRef\]](#)
10. Short, D.B. Use of 3D printing by museums: Educational exhibits, artifact education, and artifact restoration 3D. *Print. Addit. Manuf.* **2015**, *2*, 209–215. [\[CrossRef\]](#)
11. Zhao, H.; Liu, X.; Zhao, W.; Wang, G.; Liu, B. An Overview of Research on FDM 3D Printing Process of Continuous Fiber Reinforced Composites. *J. Phys. Conf. Ser.* **2019**, *1213*, 052037. [\[CrossRef\]](#)
12. De Leon, A.C.; Chen, Q.; Palaganas, N.B.; Palaganas, J.O.; Manapat, J.; Advincula, R.C. High performance polymer nanocomposites for additive manufacturing applications. *React. Funct. Polym.* **2016**, *103*, 141–155. [\[CrossRef\]](#)
13. Afrose, M.F.; Masood, S.H.; Nikzad, M.; Iovenitti, P. Effects of part build orientations on fatigue behaviour of FDM-processed PLA material. *Adv. Mater. Res.* **2014**, *1*, 21–28. [\[CrossRef\]](#)
14. Tran, P.; Ngo, T.D.; Ghazlan, A.; Hui, D. Biomaterial 3D printing and numerical analysis of bio-inspired composite structures under in-plane and transverse loadings. *Compos. Part B Eng.* **2017**, *108*, 210–223. [\[CrossRef\]](#)
15. Sharma, K.; Raghavan, J. Proceedings of the Canadian Society for Mechanical Engineering International Congress. *Can. J. Respir. Ther.* **2020**, *57*, 32–38.
16. Dawoud, M.; Taha, I.; Ebeid, S.J. Mechanical behaviour of ABS: An experimental study using FDM and injection moulding techniques. *J. Manuf. Process.* **2016**, *21*, 39–45. [\[CrossRef\]](#)
17. Ahn, S.; Montero, M.; Odell, D.; Roundy, S.; Wright, P.K. Anisotropic material properties of fused deposition modeling ABS. *Rapid Prototyp. J.* **2002**, *8*, 248–257. [\[CrossRef\]](#)
18. Kam, M.; İpekçi, A.; Şengül, Ö. Investigation of the Effect of FDM Process Parameters on Mechanical Properties of 3D Printed PA12 Samples Using Taguchi Method. *J. Thermoplast. Compos. Mater.* **2021**, 1–19. [\[CrossRef\]](#)
19. Tanikella, N.G.; Wittbrodt, B.; Pearce, J.M. Tensile strength of commercial polymer materials for fused filament fabrication 3D printing. *Addit. Manuf.* **2017**, *15*, 40–47. [\[CrossRef\]](#)
20. Angelopoulos, P.M.; Samouhos, M.; Taxiarchou, M. Functional fillers in composite filaments for fused filament fabrication; a review. *Mater. Today Proc.* **2021**, *37*, 4031–4043. [\[CrossRef\]](#)
21. Lee, C.H.; Padzil, F.N.B.M.; Lee, S.H.; Ainun, Z.M.A.; Abdullah, L.C. Potential for Natural Fiber Reinforcement in PLA Polymer Filaments for Fused Deposition Modeling (FDM) Additive Manufacturing: A Review. *Polymers* **2021**, *13*, 1407. [\[CrossRef\]](#)
22. Ju, D.; Meichun, L.; Ling, Z.; Sunyoung, L.; Changtong, M.; Xinwu, X.; Qinglin, W.J. The influence of grafted cellulose nanofibers and postextrusion annealing treatment on selected properties of poly(lactic acid) filaments for 3D printing. *Polym. Sci. Part B Polym. Phys.* **2017**, *55*, 847–885.
23. Gama, N.; Magina, S.; Barros-Timmons, A.; Ferreira, A. Enhanced Compatibility between Coconut Fibers/PP via Chemical Modification for 3D Printing. *Prog. Addit. Manuf.* **2021**, *7*, 213–223. [\[CrossRef\]](#)
24. Lin, W.; Qiuling, C.; Ying, C. Study on the properties of coffee carbon filament yarns. *Adv. Mater. Res.* **2013**, *821*, 64–67.
25. Awalluddin, D.; Mohd Ariffin, M.A.; Osman, M.H.; Hussin, M.W.; Ismail, M.A.; Lee, H.-S.; Abdul Shukor Lim, N.H. Mechanical properties of different bamboo species. *MATEC Web Conf.* **2017**, *138*, 01024. [\[CrossRef\]](#)
26. Thakur, V.K.; Thakur, M.K.; Pappu, A. *Hybrid Polymer Composite Materials: Processing*; Woodhead Publishing: Oxford, UK, 2017.
27. Chang, B.P.; Gupta, A.; Muthuraj, R.; Mekonnen, T.H. Bioresourced Fillers for Rubber Composite Sustainability: Current Development and Future Opportunities. *Green Chem.* **2021**, *23*, 5337–5378. [\[CrossRef\]](#)
28. Xanthos, M. *Functional Fillers for Plastics: Second, Updated and Enlarged Edition*; WILEY-VCH Verlag GmbH & Co. KGaA: Weinheim, Germany, 2010.
29. Xu, H.; Cheng, H.; McClements, D.J.; Chen, L.; Long, J.; Jin, Z. Enhancing the Physicochemical Properties and Functional Performance of Starch-Based Films Using Inorganic Carbon Materials: A Review. *Carbohydr. Polym.* **2022**, *295*, 119743. [\[CrossRef\]](#) [\[PubMed\]](#)
30. Bayne, S.C.; Heymann, H.O.; Swift, E.J. Update on Dental Composite Restorations. *J. Am. Dent. Assoc.* **1994**, *125*, 687–701. [\[CrossRef\]](#)
31. Wypych, G. *Handbook of Fillers*; ChemTec Publishing: Toronto, ON, Canada, 2016; Volume 938.
32. DeArmitt, C.; Rothon, R. Particulate fillers, selection and use in polymer composites. In *Encyclopedia of Polymers and Composites*; Springer: Heidelberg/Berlin, Germany, 2015; pp. 1–19.
33. Yan, Q.; Dai, W.; Gao, J.; Tan, X.; Lv, L.; Ying, J.; Lu, X.; Lu, J.; Yao, Y.; Wei, Q.; et al. Ultrahigh-Aspect-Ratio Boron Nitride Nanosheets Leading to Superhigh In-Plane Thermal Conductivity of Foldable Heat Spreader. *ACS Nano* **2021**, *15*, 6489–6498. [\[CrossRef\]](#)
34. Jan, R.; Habib, A.; Abbasi, H.Y. High Aspect Ratio Graphene Nanosheets Cause a Very Low Percolation Threshold for Polymer Nanocomposites. *Acta Phys. Pol. A* **2016**, *129*, 478–481. [\[CrossRef\]](#)
35. Yang, H.; Chen, T.; Wang, H.; Bai, S.; Guo, X. One-Pot Rapid Synthesis of High Aspect Ratio Silver Nanowires for Transparent Conductive Electrodes. *Mater. Res. Bull.* **2018**, *102*, 79–85. [\[CrossRef\]](#)

36. Liu, J.; Zhang, H.; Sun, H.; Liu, Y.; Liu, W.; Su, B.; Li, S. The Development of Filler Morphology in Dental Resin Composites: A Review. *Materials* **2021**, *14*, 5612. [\[CrossRef\]](#)
37. Harper, C.A. *Handbook of Plastics Technologies: The Complete Guide to Properties and Performance*; McGraw-Hill Companies, Inc.: New York, NY, USA, 2006.
38. Zglobicka, I.; Chmielewska, A.; Topal, E.; Kutukova, K.; Gluch, J.; Krüger, P.; Kilroy, C.; Swieszkowski, W.; Kurzydłowski, K.J.; Zschech, E. 3D Diatom—Designed and Selective Laser Melting (SLM) Manufactured Metallic Structures. *Sci. Rep.* **2019**, *9*, 19777. [\[CrossRef\]](#)
39. Nanni, A.; Messori, M. Thermo-mechanical properties and creep modelling of wine lees filled Polyamide 11 (PA11) and Polybutylene succinate (PBS) bio-composites. *Compos. Sci. Technol.* **2020**, *188*, 107974. [\[CrossRef\]](#)
40. Aggarwal, S.; Johnson, S.; Saloni, D.; Hakovirta, M. Novel 3D Printing Filament Composite Using Diatomaceous Earth and Polylactic Acid for Materials Properties and Cost Improvement. *Compos. Part B Eng.* **2019**, *177*, 107310. [\[CrossRef\]](#)
41. Han, R.; Buchanan, F.; Julius, M.; Walsh, P.J. Filament Extrusion of Bioresorbable PDLGA for Additive Manufacturing Utilising Diatom Biosilica to Inhibit Process-Induced Thermal Degradation. *J. Mech. Behav. Biomed. Mater.* **2021**, *116*, 104265. [\[CrossRef\]](#) [\[PubMed\]](#)
42. Han, R.; Buchanan, F.; Ford, L.; Julius, M.; Walsh, P.J. A Comparison of the Degradation Behaviour of 3D Printed PDLGA Scaffolds Incorporating Bioglass or Biosilica. *Mater. Sci. Eng. C* **2021**, *120*, 111755. [\[CrossRef\]](#) [\[PubMed\]](#)
43. Dobrosielska, M.; Przekop, R.; Sztorch, B.; Brząkański, D.; Zglobicka, I.; Łepicka, M.; Dobosz, R.; Kurzydłowski, K. Biogenic Composite Filaments Based on Polylactide and Diatomaceous Earth for 3D Printing. *Materials* **2020**, *13*, 4632. [\[CrossRef\]](#)
44. Rodríguez-Blanco, J.D.; Shaw, S.; Benning, L.G. The Kinetics and Mechanisms of Amorphous Calcium Carbonate (ACC) Crystallization to Calcite, Viavaterite. *Nanoscale* **2011**, *3*, 265–271. [\[CrossRef\]](#)
45. Shafiur Rahman, G.M.; Aftab, H.; Shariful Islam, M.; Mukhlis, M.Z.B.; Ali, F. Enhanced Physico-Mechanical Properties of Polyester Resin Film Using CaCO₃ Filler. *Fibers Polym.* **2016**, *17*, 59–65. [\[CrossRef\]](#)
46. Adeosun, S.O.; Usman, M.A.; Akpan, E.I.; Dibia, W.I. Characterization of LDPE Reinforced with Calcium Carbonate—Fly Ash Hybrid Filler. *J. Miner. Mater. Charact. Eng.* **2014**, *02*, 334–345. [\[CrossRef\]](#)
47. Donate, R.; Monzón, M.; Alemán-Domínguez, M.E.; Ortega, Z. Enzymatic Degradation Study of PLA-Based Composite Scaffolds. *Rev. Adv. Mater. Sci.* **2020**, *59*, 170–175. [\[CrossRef\]](#)
48. Dong, M.; Qu, C.; Zhang, S.; Chou, B.; Gao, D. Application of PP in fused deposition modeling process. *China Synth. Resin Plast.* **2019**, *36*, 23–30.
49. Zárybnická, L.; Ševčík, R.; Pokorný, J.; Machová, D.; Stránská, E.; Šál, J. CaCO₃ Polymorphs Used as Additives in Filament Production for 3D Printing. *Polymers* **2022**, *14*, 199. [\[CrossRef\]](#) [\[PubMed\]](#)
50. Shang, W.; Liu, Q.; He, E.; Chen, S. Study on Properties of Polymers Packed by Aragonite Whisker. In Proceedings of the 6th International Conference on Properties and Applications of Dielectric Materials, Xi'an, China, 21–26 June 2000; Volume 2, p. 431.
51. Lin, Y.; Chen, H.; Chan, C.-M.; Wu, J. Effects of coating amount and particle concentration on the impact toughness of polypropylene/CaCO₃ nanocomposites. *Eur. Polym. J.* **2011**, *47*, 294–304. [\[CrossRef\]](#)
52. Yang, K.; Yang, Q.; Li, G.; Zhang, Y.; Zhang, P. Mechanical Properties and Morphologies of Polypropylene/Single-Filler or Hybrid-Filler Calcium Carbonate Composites. *Polym. Eng. Sci.* **2007**, *47*, 95–102. [\[CrossRef\]](#)
53. Sudeepan, J.; Kumar, K.; Barman, T.K.; Sahoo, P. Study of Tribological Behavior of ABS/CaCO₃ Composite Using Grey Relational Analysis. *Procedia Mater. Sci.* **2014**, *6*, 682–691. [\[CrossRef\]](#)
54. Kotlarz, M.; Jordan, R.; Wegner, E.; Dobrzyński, P.; Neunzehn, J.; Lederer, A.; Wolf-Brandstetter, C.; Pamula, E.; Scharnweber, D. One step 3D printing of surface functionalized composite scaffolds for tissue engineering applications. *Acta Bioeng. Biomech.* **2018**, *20*, 35–45. [\[PubMed\]](#)
55. Varga, P.; Lorinczy, D.; Toth, L.; Pentek, A.; Nyitrai, M.; Maroti, P. Novel PLA-CaCO₃ Composites in Additive Manufacturing of Upper Limb Casts and Orthotics—A Feasibility Study. *Mater. Res. Express* **2019**, *6*, 045317. [\[CrossRef\]](#)
56. Kasuga, T.; Maeda, H.; Kato, K.; Nogami, M.; Hata, K.; Ueda, M. Preparation of Poly(Lactic Acid) Composites Containing Calcium Carbonate (Vaterite). *Biomaterials* **2003**, *24*, 3247–3253. [\[CrossRef\]](#)
57. Castilho, M.; Moseke, C.; Ewald, A.; Gbureck, U.; Groll, J.; Pires, I.; Teßmar, J.; Vorndran, E. Direct 3D Powder Printing of Biphasic Calcium Phosphate Scaffolds for Substitution of Complex Bone Defects. *Biofabrication* **2014**, *6*, 015006. [\[CrossRef\]](#)
58. Tymrak, B.M.; Kreiger, M.; Pearce, J.M. Mechanical Properties of Components Fabricated with Open-Source 3-D Printers under Realistic Environmental Conditions. *Mater. Des.* **2014**, *58*, 242–246. [\[CrossRef\]](#)
59. Gang, F.; Ye, W.; Ma, C.; Wang, W.; Xiao, Y.; Liu, C.; Sun, X. 3D Printing of PLLA/Biomaterial Composite Bone Tissue Engineering Scaffolds. *Materials* **2022**, *15*, 4280. [\[CrossRef\]](#)
60. Neumann, R.; Neunzehn, J.; Hinueber, C.; Flath, T.; Schulze, F.P.; Wiesmann, H.-P. 3D-Printed Poly-ε-Caprolactone-CaCO₃-Biocomposite-Scaffolds for Hard Tissue Regeneration. *Express Polym. Lett.* **2019**, *13*, 2–17. [\[CrossRef\]](#)
61. Babilotte, J.; Guduric, V.; Le Nihouannen, D.; Naveau, A.; Fricain, J.-C.; Catros, S. 3D Printed Polymer-Mineral Composite Biomaterials for Bone Tissue Engineering: Fabrication and Characterization. *J. Biomed. Mater. Res. Part B Appl. Biomater.* **2019**, *107*, 2579–2595. [\[CrossRef\]](#) [\[PubMed\]](#)
62. Wang, Y.; Zhou, Y.; Lin, L.; Corker, J.; Fan, M. Overview of 3D Additive Manufacturing (AM) and Corresponding AM Composites. *Compos. Part A Appl. Sci. Manuf.* **2020**, *139*, 106114. [\[CrossRef\]](#)

63. Shanmugam, V.; Rajendran, D.J.J.; Babu, K.; Rajendran, S.; Veerasimman, A.; Marimuthu, U.; Singh, S.; Das, O.; Neisiany, R.E.; Hedenqvist, M.S.; et al. The Mechanical Testing and Performance Analysis of Polymer-Fibre Composites Prepared through the Additive Manufacturing. *Polym. Test.* **2021**, *93*, 106925. [\[CrossRef\]](#)
64. Subramaniam, M.; Karuppan, S.; Eswaran, P.; Appusamy, A.; Naveen Shankar, A. State of Art on Fusion Deposition Modeling Machines Process Parameter Optimization on Composite Materials. *Mater. Today Proc.* **2021**, *45*, 820–827. [\[CrossRef\]](#)
65. Muthe, L.P.; Pickering, K.; Gauss, C. A Review of 3D/4D Printing of Poly-Lactic Acid Composites with Bio-Derived Reinforcements. *Compos. Part C Open Access* **2022**, *8*, 100271. [\[CrossRef\]](#)
66. Khalifa, M.; Anandhan, S.; Wuzella, G.; Lammer, H.; Mahendran, A.R. Thermoplastic Polyurethane Composites Reinforced with Renewable and Sustainable Fillers—A Review. *Polym.-Plast. Technol. Mater.* **2020**, *59*, 1751–1769. [\[CrossRef\]](#)
67. Suárez, L.; Castellano, J.; Díaz, S.; Tcharkhtchi, A.; Ortega, Z. Are Natural-Based Composites Sustainable? *Polymers* **2021**, *13*, 2326. [\[CrossRef\]](#)
68. Rajak, D.K.; Pagar, D.D.; Menezes, P.L.; Linul, E. Fiber-Reinforced Polymer Composites: Manufacturing, Properties, and Applications. *Polymers* **2019**, *11*, 1667. [\[CrossRef\]](#)
69. Mohan, N.; Senthil, P.; Vinodh, S.; Jayanth, N. A Review on Composite Materials and Process Parameters Optimisation for the Fused Deposition Modelling Process. *Virtual Phys. Prototyp.* **2017**, *12*, 47–59. [\[CrossRef\]](#)
70. Ilyas, R.A.; Sapuan, S.M.; Harussani, M.M.; Hakimi, M.Y.A.Y.; Haziq, M.Z.M.; Atikah, M.S.N.; Asyraf, M.R.M.; Ishak, M.R.; Razman, M.R.; Nurazzi, N.M.; et al. Polylactic Acid (PLA) Biocomposite: Processing, Additive Manufacturing and Advanced Applications. *Polymers* **2021**, *13*, 1326. [\[CrossRef\]](#) [\[PubMed\]](#)
71. Badgar, K.; Abdalla, N.; El-Ramady, H.; Prokisch, J. Sustainable Applications of Nanofibers in Agriculture and Water Treatment: A Review. *Sustainability* **2022**, *14*, 464. [\[CrossRef\]](#)
72. Wasti, S.; Adhikari, S. Use of Biomaterials for 3D Printing by Fused Deposition Modeling Technique: A Review. *Front. Chem.* **2020**, *8*, 315. [\[CrossRef\]](#) [\[PubMed\]](#)
73. Velu, R.; Raspall, F.; Singamneni, S. 3D Printing Technologies and Composite Materials for Structural Applications. In *Green Composites for Automotive Applications*; Koronis, G., Silva, A., Eds.; Woodhead Publishing: Duxford, UK, 2019; pp. 171–196.
74. Murawski, A.; Diaz, R.; Inglesby, S.; Delabar, K.; Quirino, R.L. Synthesis of Bio-Based Polymer Composites: Fabrication, Fillers, Properties, and Challenges. *Lect. Notes Bioeng.* **2019**, 29–55. [\[CrossRef\]](#)
75. Gharde, S.; Surendren, A.; Korde, J.M.; Saini, S.; Deoray, N.; Goud, R.; Nimje, S.; Kandasubramanian, B. Recent Advances in Additive Manufacturing of Bio-Inspired Materials. In *Biomufacturing*; Prakash, C., Singh, S., Singh, R., Ramakrishna, S., Pabla, B.S., Puri, S., Uddin, M.S., Eds.; Springer: Cham, Switzerland, 2019; pp. 35–68.
76. Le Duigou, A.; Correa, D.; Ueda, M.; Matsuzaki, R.; Castro, M. A Review of 3D and 4D Printing of Natural Fibre Biocomposites. *Mater. Des.* **2020**, *194*, 108911. [\[CrossRef\]](#)
77. Zhao, X.; Copenhaver, K.; Wang, L.; Korey, M.; Gardner, D.J.; Li, K.; Lamm, M.E.; Kishore, V.; Bhagia, S.; Tajvidi, M.; et al. Recycling of Natural Fiber Composites: Challenges and Opportunities. *Resour. Conserv. Recycl.* **2022**, *177*, 105962. [\[CrossRef\]](#)
78. Balla, V.K.; Kate, K.H.; Satyavolu, J.; Singh, P.; Tadimet, J.G.D. Additive Manufacturing of Natural Fiber Reinforced Polymer Composites: Processing and Prospects. *Compos. Part B Eng.* **2019**, *174*, 106956. [\[CrossRef\]](#)
79. Li, M.; Pu, Y.; Thomas, V.M.; Yoo, C.G.; Ozcan, S.; Deng, Y.; Nelson, K.; Ragauskas, A.J. Recent Advancements of Plant-Based Natural Fiber-Reinforced Composites and Their Applications. *Compos. Part B Eng.* **2020**, *200*, 108254. [\[CrossRef\]](#)
80. Tonk, R. Natural Fibers for Sustainable Additive Manufacturing: A State of the Art Review. *Mater. Today Proc.* **2020**, *37*, 3087–3090. [\[CrossRef\]](#)
81. Deb, D.; Jafferson, J.M. Natural Fibers Reinforced FDM 3D Printing Filaments. *Mater. Today Proc.* **2021**, *46*, 1308–1318. [\[CrossRef\]](#)
82. Ganguly, A.; Shankar, S.; Das, A.; Shukla, M.; Swaroop, C.; Bhardwaj, T. Natural Fibre Reinforced Composites: A Review Based on Additive Manufacturing Routes and Biodegradability Perspective. *Mater. Today Proc.* **2022**, *62*, 131–135. [\[CrossRef\]](#)
83. Kopparthi, S.D.S.; Netravali, A.N. Review: Green Composites for Structural Applications. *Compos. Part C Open Access* **2021**, *6*, 100169. [\[CrossRef\]](#)
84. Mangat, A.S.; Singh, S.; Gupta, M.; Sharma, R. Experimental Investigations on Natural Fiber Embedded Additive Manufacturing-Based Biodegradable Structures for Biomedical Applications. *Rapid Prototyp. J.* **2018**, *24*, 1221–1234. [\[CrossRef\]](#)
85. Sekar, V.; Fouladi, M.H.; Namasivayam, S.N.; Sivanesan, S. Additive Manufacturing: A Novel Method for Developing an Acoustic Panel Made of Natural Fiber-Reinforced Composites with Enhanced Mechanical and Acoustical Properties. *J. Eng.* **2019**, *2019*, 4546863. [\[CrossRef\]](#)
86. Mazzanti, V.; Mollica, F. A Review of Wood Polymer Composites Rheology and Its Implications for Processing. *Polymers* **2020**, *12*, 2304. [\[CrossRef\]](#)
87. Suriani, M.J.; Ilyas, R.A.; Zuhri, M.Y.M.; Khalina, A.; Sultan, M.T.H.; Sapuan, S.M.; Ruzaidi, C.M.; Wan, F.N.; Zulkifli, F.; Harussani, M.M.; et al. Critical Review of Natural Fiber Reinforced Hybrid Composites: Processing, Properties, Applications and Cost. *Polymers* **2021**, *13*, 3514. [\[CrossRef\]](#)
88. Shahinur, S.; Sayeed, M.M.A.; Hasan, M.; Sayem, A.S.M.; Haider, J.; Ura, S. Current Development and Future Perspective on Natural Jute Fibers and Their Biocomposites. *Polymers* **2022**, *14*, 1445. [\[CrossRef\]](#)
89. Rajendran Royan, N.R.; Leong, J.S.; Chan, W.N.; Tan, J.R.; Shamsuddin, Z.S.B. Current State and Challenges of Natural Fibre-Reinforced Polymer Composites as Feeder in FDM-Based 3D Printing. *Polymers* **2021**, *13*, 2289. [\[CrossRef\]](#)

90. Ahmed, W.; Alnajjar, F.; Zanelidin, E.; Al-Marzouqi, A.H.; Gochoo, M.; Khalid, S. Implementing FDM 3D Printing Strategies Using Natural Fibers to Produce Biomass Composite. *Materials* **2020**, *13*, 4065. [\[CrossRef\]](#)
91. Aida, H.J.; Nadlene, R.; Mastura, M.T.; Yusriah, L.; Sivakumar, D.; Ilyas, R.A. Natural Fibre Filament for Fused Deposition Modelling (FDM): A Review. *Int. J. Sustain. Eng.* **2021**, *14*, 1988–2008. [\[CrossRef\]](#)
92. Devarajan, B.; LakshmiNarasimhan, R.; Venkateswaran, B.; Mavinkere Rangappa, S.; Siengchin, S. Additive Manufacturing of Jute Fiber Reinforced Polymer Composites: A Concise Review of Material Forms and Methods. *Polym. Compos.* **2022**, *46*, 1308–1318. [\[CrossRef\]](#)
93. Rajeshkumar, G.; Arvinth Seshadri, S.; Devnani, G.L.; Sanjay, M.R.; Siengchin, S.; Prakash Maran, J.; Al-Dhabi, N.A.; Karuppiah, P.; Mariadhas, V.A.; Sivarajasekar, N.; et al. Environment Friendly, Renewable and Sustainable Poly Lactic Acid (PLA) Based Natural Fiber Reinforced Composites—A Comprehensive Review. *J. Clean. Prod.* **2021**, *310*, 127483. [\[CrossRef\]](#)
94. Palmqvist, E.; Hahn-Hägerdal, B. Fermentation of Lignocellulosic Hydrolysates. II: Inhibitors and Mechanisms of Inhibition. *Bioresour. Technol.* **2000**, *74*, 25–33. [\[CrossRef\]](#)
95. Mastura, M.T.; Nadlene, R.; Jumaidin, R.; Kudus, S.A.; Mansor, M.R.; Firdaus, H.M.S. Concurrent Material Selection of Natural Fibre Filament for Fused Deposition Modeling Using Integration of Analytic Hierarchy Process/Analytic Network Process. *J. Renew. Mater.* **2022**, *10*, 1221–1238. [\[CrossRef\]](#)
96. Le Duigou, A.; Fruleux, T.; Matsuzaki, R.; Chabaud, G.; Ueda, M.; Castro, M. 4D Printing of Continuous Flax-Fibre Based Shape-Changing Hygromorph Biocomposites: Towards Sustainable Metamaterials. *Mater. Des.* **2021**, *211*, 110158. [\[CrossRef\]](#)
97. Fruleux, T.; Castro, M.; Sauleau, P.; Matsuzaki, R.; Le Duigou, A. Matrix Stiffness: A Key Parameter to Control Hydro-Elasticity and Morphing of 3D Printed Biocomposite. *Compos. Part A Appl. Sci. Manuf.* **2022**, *156*, 106882. [\[CrossRef\]](#)
98. Le Duigou, A.; Chabaud, G.; Matsuzaki, R.; Castro, M. Tailoring the Mechanical Properties of 3D-Printed Continuous Flax/PLA Biocomposites by Controlling the Slicing Parameters. *Compos. Part B Eng.* **2020**, *203*, 108474. [\[CrossRef\]](#)
99. Stoof, D.; Pickering, K.; Zhang, Y. Fused Deposition Modelling of Natural Fibre/Polylactic Acid Composites. *J. Compos. Sci.* **2017**, *1*, 8. [\[CrossRef\]](#)
100. Yaguchi, Y.; Takeuchi, K.; Waragai, T.; Tateno, T. Durability Evaluation of an Additive Manufactured Biodegradable Composite with Continuous Natural Fiber in Various Conditions Reproducing Usage Environment. *Int. J. Autom. Technol.* **2020**, *14*, 959–965. [\[CrossRef\]](#)
101. Cai, R.; Lin, H.; Cheng, P.; Zhang, Z.; Wang, K.; Peng, Y.; Wu, Y.; Ahzi, S. Investigation on Dynamic Strength of 3D-Printed Continuous Ramie Fiber Reinforced Biocomposites at Various Strain Rates Using Machine Learning Methods. *Polym. Compos.* **2022**, *43*, 5235–5249. [\[CrossRef\]](#)
102. Regalla, S.P.; Karwa, S.S.; Rajesh, S.; Shyam, P.V.; Shrivastava, P.N. Strength and Fracture Behaviour of Polymer Matrix Composite Layered Structures Made by Additive Manufacturing. *Mater. Today Proc.* **2020**, *28*, 1030–1038. [\[CrossRef\]](#)
103. Jamadi, A.H.; Razali, N.; Petru, M.; Taha, M.M.; Muhammad, N.; Ilyas, R.A. Effect of Chemically Treated Kenaf Fibre on Mechanical and Thermal Properties of PLA Composites Prepared through Fused Deposition Modeling (FDM). *Polymers* **2021**, *13*, 3299. [\[CrossRef\]](#) [\[PubMed\]](#)
104. Taborda-Ríos, J.A.; López-Botello, O.; Zambrano-Robledo, P.; Reyes-Osorio, L.A.; Garza, C. Mechanical Characterisation of a Bamboo Fibre/Polylactic Acid Composite Produced by Fused Deposition Modelling. *J. Reinf. Plast. Compos.* **2020**, *39*, 932–944. [\[CrossRef\]](#)
105. Rafiee, M.; Abidnejad, R.; Ranta, A.; Ojha, K.; Karakoç, A.; Paltakari, J. Exploring the Possibilities of FDM Filaments Comprising Natural Fiber-Reinforced Biocomposites for Additive Manufacturing. *AIMS Mater. Sci.* **2021**, *8*, 524–537. [\[CrossRef\]](#)
106. Dogru, A.; Sozen, A.; Neser, G.; Seydibeyoglu, M.O. Effects of Aging and Infill Pattern on Mechanical Properties of Hemp Reinforced PLA Composite Produced by Fused Filament Fabrication (FFF). *Appl. Sci. Eng. Prog.* **2021**, *14*, 651–660. [\[CrossRef\]](#)
107. Kesentini, Z.; El Mahi, A.; Rebiere, J.-L.; El Guerjouma, R.; Beyaoui, M.; Haddar, M. Effect of Hydric Aging on the Static and Vibration Behavior of 3D Printed Bio-Based Flax Fiber Reinforced Poly-Lactic Acid Composites. *Polym. Polym. Compos.* **2022**, *30*, 09673911221081826. [\[CrossRef\]](#)
108. Mazur, K.E.; Borucka, A.; Kaczor, P.; Gadek, S.; Bogucki, R.; Mirzewiński, D.; Kuciel, S. Mechanical, Thermal and Microstructural Characteristic of 3D Printed Polylactide Composites with Natural Fibers: Wood, Bamboo and Cork. *J. Polym. Environ.* **2021**, *30*, 2341–2354. [\[CrossRef\]](#)
109. Mangat, A.S.; Singh, S. Characterization of Natural Fibre-Embedded Biodegradable Porous Structures Prepared with Fused Deposition Process. *J. Thermoplast. Compos. Mater.* **2018**, *32*, 761–777. [\[CrossRef\]](#)
110. Sekar, V.; Eh Noum, S.Y.; Sivanesan, S.; Putra, A.; Kassim, D.H.; Wong, Y.S.; Chin, K.C. Effect of Perforation Volume on Acoustic Absorption of the 3D Printed Micro-Perforated Panels Made of Polylactic Acid Reinforced with Wood Fibers. *J. Phys. Conf. Ser.* **2021**, *2120*, 012039. [\[CrossRef\]](#)
111. Sekar, V.; Eh Noum, S.Y.; Sivanesan, S.; Putra, A.; Chin Vui Sheng, D.D.; Kassim, D.H. Effect of Thickness and Infill Density on Acoustic Performance of 3D Printed Panels Made of Natural Fiber Reinforced Composites. *J. Nat. Fibers* **2021**, 1–9. [\[CrossRef\]](#)
112. Balla, V.K.; Tadimetri, J.G.D.; Kate, K.H.; Satyavolu, J. 3D Printing of Modified Soybean Hull Fiber/Polymer Composites. *Mater. Chem. Phys.* **2020**, *254*, 123452. [\[CrossRef\]](#)
113. Ariel Leong, J.J.; Koay, S.C.; Chan, M.Y.; Choo, H.L.; Tshai, K.Y.; Ong, T.K. Composite Filament Made from Post-Used Styrofoam and Corn Husk Fiber for Fuse Deposition Modeling. *J. Nat. Fibers* **2021**, 1–16. [\[CrossRef\]](#)

114. Costa, I.L.; Pereira, P.H.; Claro, A.M.; Amaral, N.C.D.; Barud, H.d.S.; Ribeiro, R.B.; Mulinari, D.R. 3D-Printing Pen from Valorization of Pine Cone Residues as Reinforcement in Acrylonitrile Butadiene Styrene (ABS): Microstructure and Thermal Properties. *J. Thermoplast. Compos. Mater.* **2021**, 1–20. [\[CrossRef\]](#)
115. Ahmad, M.N.; Wahid, M.K.; Maidin, N.A.; Ab Rahman, M.H.; Osman, M.H.; Alis@Elias, I.F. Mechanical Characteristics of Oil Palm Fiber Reinforced Thermoplastics as Filament for Fused Deposition Modeling (FDM). *Adv. Manuf.* **2020**, *8*, 72–81. [\[CrossRef\]](#)
116. Han, S.N.M.F.; Taha, M.M.; Mansor, M.R.; Rahman, M.A.A. Investigation of Tensile and Flexural Properties of Kenaf Fiber-Reinforced Acrylonitrile Butadiene Styrene Composites Fabricated by Fused Deposition Modeling. *J. Eng. Appl. Sci.* **2022**, *69*, 52. [\[CrossRef\]](#)
117. Balla, V.K.; Tadimet, J.G.D.; Sudan, K.; Satyavolu, J.; Kate, K.H. First Report on Fabrication and Characterization of Soybean Hull Fiber: Polymer Composite Filaments for Fused Filament Fabrication. *Prog. Addit. Manuf.* **2020**, *6*, 39–52. [\[CrossRef\]](#)
118. Carrete, I.A.; Quiñonez, P.A.; Bermudez, D.; Roberson, D.A. Incorporating Textile-Derived Cellulose Fibers for the Strengthening of Recycled Polyethylene Terephthalate for 3D Printing Feedstock Materials. *J. Polym. Environ.* **2020**, *29*, 662–671. [\[CrossRef\]](#)
119. Morales, M.; Atencio Martinez, C.; Maranon, A.; Hernandez, C.; Michaud, V.; Porras, A. Development and Characterization of Rice Husk and Recycled Polypropylene Composite Filaments for 3D Printing. *Polymers* **2021**, *13*, 1067. [\[CrossRef\]](#) [\[PubMed\]](#)
120. Morales, M.A.; Maranon, A.; Hernandez, C.; Porras, A. Development and Characterization of a 3D Printed Cocoa Bean Shell Filled Recycled Polypropylene for Sustainable Composites. *Polymers* **2021**, *13*, 3162. [\[CrossRef\]](#)
121. Tao, Y.; Wang, H.; Li, Z.; Li, P.; Shi, S.Q. Development and Application of Wood Flour-Filled Polylactic Acid Composite Filament for 3D Printing. *Materials* **2017**, *10*, 339. [\[CrossRef\]](#)
122. Xie, G.; Zhang, Y.; Lin, W. Plasticizer Combinations and Performance of Wood Flour–Poly(Lactic Acid) 3D Printing Filaments. *BioResources* **2017**, *12*, 6736–6748. [\[CrossRef\]](#)
123. Bi, H.; Ren, Z.; Guo, R.; Xu, M.; Song, Y. Fabrication of Flexible Wood Flour/Thermoplastic Polyurethane Elastomer Composites Using Fused Deposition Molding. *Ind. Crop Prod.* **2018**, *122*, 76–84. [\[CrossRef\]](#)
124. Kariz, M.; Sernek, M.; Obućina, M.; Kuzman, M.K. Effect of Wood Content in FDM Filament on Properties of 3D Printed Parts. *Mater. Today Commun.* **2018**, *14*, 135–140. [\[CrossRef\]](#)
125. Le Guen, M.-J.; Hill, S.; Smith, D.; Theobald, B.; Gaugler, E.; Barakat, A.; Mayer-Laigle, C. Influence of Rice Husk and Wood Biomass Properties on the Manufacture of Filaments for Fused Deposition Modeling. *Front. Chem.* **2019**, *7*, 735. [\[CrossRef\]](#)
126. Tran, T.N.; Bayer, I.S.; Heredia-Guerrero, J.A.; Frugone, M.; Lagomarsino, M.; Maggio, F.; Athanassiou, A. Cocoa Shell Waste Biofilaments for 3D Printing Applications. *Macromol. Mater. Eng.* **2017**, *302*, 1700219. [\[CrossRef\]](#)
127. Girdis, J.; Gaudion, L.; Proust, G.; Löschke, S.; Dong, A. Rethinking Timber: Investigation into the Use of Waste Macadamia Nut Shells for Additive Manufacturing. *JOM* **2016**, *69*, 575–579. [\[CrossRef\]](#)
128. Brites, F.; Malça, C.; Gaspar, F.; Horta, J.F.; Franco, M.C.; Biscaia, S.; Mateus, A. Cork Plastic Composite Optimization for 3D Printing Applications. *Procedia Manuf.* **2017**, *12*, 156–165. [\[CrossRef\]](#)
129. Gnanamani Sankaravel, S.; Syed, R.B.; Manivachakan, V. In Vitro and Mechanical Characterization of PLA/Egg Shell Biocomposite Scaffold Manufactured Using F Used Deposition Modeling Technology for Tissue Engineering Applications. *Polym. Compos.* **2021**, *43*, 173–186. [\[CrossRef\]](#)
130. Flores-Hernandez, C.G.; Velasco-Santos, C.; Hernandez-Zea, A.L.; Gomez-Guzman, O.; Yañez-Limon, J.M.; Rivera-Armenta, J.L.; Martinez-Hernandez, A.L. Low Concentrations for Significant Improvements in Thermal and Thermomechanical Properties of Poly(Lactic Acid)–Keratin Biocomposites Obtained by Extrusion and 3D Printing. *J. Nat. Fibers* **2020**, *19*, 1715–1728. [\[CrossRef\]](#)
131. Scaffaro, R.; Maio, A.; Gulino, E.F.; Alaimo, G.; Morreale, M. Green Composites Based on PLA and Agricultural or Marine Waste Prepared by FDM. *Polymers* **2021**, *13*, 1361. [\[CrossRef\]](#)
132. Martin, O.; Avérous, L. Poly(Lactic Acid): Plasticization and Properties of Biodegradable Multiphase Systems. *Polymer* **2001**, *42*, 6209–6219. [\[CrossRef\]](#)
133. Huneault, M.A.; Li, H. Morphology and Properties of Compatibilized Polylactide/Thermoplastic Starch Blends. *Polymer* **2007**, *48*, 270–280. [\[CrossRef\]](#)
134. Zhou, L.; Zhao, G.; Feng, Y.; Yin, J.; Jiang, W. Toughening Polylactide with Polyether-Block-Amide and Thermoplastic Starch Acetate: Influence of Starch Esterification Degree. *Carbohydr. Polym.* **2015**, *127*, 79–85. [\[CrossRef\]](#)
135. Hossain, M.I.; Chowdhury, M.A.; Zahid, M.S.; Sakib-Uz-Zaman, C.; Rahaman, M.L.; Kowser, M.A. Development and Analysis of Nanoparticle Infused Plastic Products Manufactured by Machine Learning Guided 3D Printer. *Polym. Test.* **2021**, *106*, 107429. [\[CrossRef\]](#)
136. Olam, M.; Tosun, N. 3D-Printed Polylactide/Hydroxyapatite/Titania Composite Filaments. *Mater. Chem. Phys.* **2022**, *276*, 125267. [\[CrossRef\]](#)
137. Singh, R.; Kumar, R.; Mascolo, I.; Modano, M. On the Applicability of Composite PA6-TiO₂ Filaments for the Rapid Prototyping of Innovative Materials and Structures. *Compos. Part B Eng.* **2018**, *143*, 132–140. [\[CrossRef\]](#)
138. Soundararajan, R.; Jayasuriya, N.; Girish Vishnu, R.G.; Guru Prasad, B.; Pradeep, C. Appraisal of Mechanical and Tribological Properties on PA6-TiO₂ Composites through Fused Deposition Modelling. *Mater. Today Proc.* **2019**, *18*, 2394–2402. [\[CrossRef\]](#)
139. Kumar Tiwary, V.; Arunkumar, P.; Kulkarni, P.M. Micro-Particle Grafted Eco-Friendly Polymer Filaments for 3D Printing Technology. *Mater. Today Proc.* **2020**, *28*, 1980–1984. [\[CrossRef\]](#)
140. Vidakis, N.; Petousis, M.; Maniadi, A.; Koudoumas, E.; Liebscher, M.; Tzounis, L. Mechanical Properties of 3D-Printed Acrylonitrile–Butadiene–Styrene TiO₂ and ATO Nanocomposites. *Polymers* **2020**, *12*, 1589. [\[CrossRef\]](#)

141. Vidakis, N.; Petousis, M.; Velidakis, E.; Tzounis, L.; Mountakis, N.; Kechagias, J.; Grammatikos, S. Optimization of the Filler Concentration on Fused Filament Fabrication 3D Printed Polypropylene with Titanium Dioxide Nanocomposites. *Materials* **2021**, *14*, 3076. [\[CrossRef\]](#)
142. Car, F.; Brnadić, G.; Tomašić, V.; Vrsaljko, D. Advanced Preparation Method of Monolithic Catalyst Carriers Using 3D-Printing Technology. *Prog. Addit. Manuf.* **2022**, *7*, 797–808. [\[CrossRef\]](#)
143. Sevastaki, M.; Suche, M.P.; Kenanakis, G. 3D Printed Fully Recycled TiO₂-Polystyrene Nanocomposite Photocatalysts for Use against Drug Residues. *Nanomaterials* **2020**, *10*, 2144. [\[CrossRef\]](#) [\[PubMed\]](#)
144. Viskadourakis, Z.; Sevastaki, M.; Kenanakis, G. 3D Structured Nanocomposites by FDM Process: A Novel Approach for Large-Scale Photocatalytic Applications. *Appl. Phys. A* **2018**, *124*, 585. [\[CrossRef\]](#)
145. Sangiorgi, A.; Gonzalez, Z.; Ferrandez-Montero, A.; Yus, J.; Sanchez-Herencia, A.J.; Galassi, C.; Sanson, A.; Ferrari, B. 3D Printing of Photocatalytic Filters Using a Biopolymer to Immobilize TiO₂ Nanoparticles. *J. Electrochem. Soc.* **2019**, *166*, H3239–H3248. [\[CrossRef\]](#)
146. Zhou, R.; Han, R.; Bingham, M.; O'Rourke, C.; Mills, A. 3D printed, plastic photocatalytic flow reactors for water purification. *Photochem. Photobiol. Sci.* **2022**, *21*, 1585–1600. [\[CrossRef\]](#)
147. Li, K.; de Rancourt de Mimérand, Y.; Jin, X.; Yi, J.; Guo, J. Metal Oxide (ZnO and TiO₂) and Fe-Based Metal–Organic-Framework Nanoparticles on 3D-Printed Fractal Polymer Surfaces for Photocatalytic Degradation of Organic Pollutants. *ACS Appl. Nano Mater.* **2020**, *3*, 2830–2845. [\[CrossRef\]](#)
148. McQueen, A.D.; Ballentine, M.L.; May, L.R.; Laber, C.H.; Das, A.; Bortner, M.J.; Kennedy, A.J. Photocatalytic Degradation of Polycyclic Aromatic Hydrocarbons in Water by 3D Printed TiO₂ Composites. *ACS EST Water* **2021**, *2*, 137–147. [\[CrossRef\]](#)
149. Kumar, S.; Singh, R.; Singh, M.; Singh, T.; Batish, A. Multi Material 3D Printing of PLA-PA6/TiO₂ Polymeric Matrix: Flexural, Wear and Morphological Properties. *J. Thermoplast. Compos. Mater.* **2020**, 1–20. [\[CrossRef\]](#)
150. Nájera, S.E.; Michel, M.; Kim, N.-S. 3D Printed PLA/PCL/TiO₂ Composite for Bone Replacement and Grafting. *MRS Adv.* **2018**, *3*, 2373–2378. [\[CrossRef\]](#)
151. Brounstein, Z.; Yeager, C.M.; Labouriau, A. Development of Antimicrobial PLA Composites for Fused Filament Fabrication. *Polymers* **2021**, *13*, 580. [\[CrossRef\]](#)
152. Horst, D.J.; Tebcherani, S.M.; Kubaski, E.T.; de Almeida Vieira, R. Bioactive Potential of 3D-Printed Oleo-Gum-Resin Disks: *B. Papyrifera*, *C. Myrrha*, and *S. Benzoin* Loading Nanooxides—TiO₂, P25, Cu₂O, and MoO₃. *Bioinorg. Chem. Appl.* **2017**, *2017*, 6398167. [\[CrossRef\]](#) [\[PubMed\]](#)
153. Ding, L.; Lu, W.; Zhang, J.; Yang, C.; Wu, G. Preparation and Performance Evaluation of Duotone 3D-Printed Polyetheretherketone as Oral Prosthetic Materials: A Proof-of-Concept Study. *Polymers* **2021**, *13*, 1949. [\[CrossRef\]](#) [\[PubMed\]](#)
154. Dong, E.; Zhao, Z.; Wang, M.; Xie, Y.; Li, S.; Shao, P.; Cheng, L.; Xu, R.X. Three-Dimensional Fuse Deposition Modeling of Tissue-Simulating Phantom for Biomedical Optical Imaging. *J. Biomed. Opt.* **2015**, *20*, 121311. [\[CrossRef\]](#)
155. Castro, J.; Rojas, E.; Ross, A.; Weller, T.; Wang, J. High-k and Low-Loss Thermoplastic Composites for Fused Deposition Modeling and Their Application to 3D-Printed Ku-Band Antennas. In Proceedings of the 2016 IEEE MTT-S International Microwave Symposium (IMS), San Francisco, CA, USA, 22–27 May 2016.
156. Castro, J.; Rojas-Nastrucci, E.A.; Ross, A.; Weller, T.M.; Wang, J. Fabrication, Modeling, and Application of Ceramic-Thermoplastic Composites for Fused Deposition Modeling of Microwave Components. *IEEE Trans. Microw. Theory Tech.* **2017**, *65*, 2073–2084. [\[CrossRef\]](#)
157. Li, H.; Watson, J.C. Continuous Glass Fibers for Reinforcement. *Encycl. Glass Sci. Technol. Hist. Cult.* **2021**, *1*, 95–109.
158. Jones, F.R.; Huff, N.T. The Structure and Properties of Glass Fibers. In *Handbook of Properties of Textile and Technical Fibres*, 2nd ed.; Bunsell, A.R., Ed.; Woodhead Publishing: Duxford, UK, 2018; pp. 757–803.
159. Goh, G.D.; Dikshit, V.; Nagalingam, A.P.; Goh, G.L.; Agarwala, S.; Sing, S.L.; Wei, J.; Yeong, W.Y. Characterization of Mechanical Properties and Fracture Mode of Additively Manufactured Carbon Fiber and Glass Fiber Reinforced Thermoplastics. *Mater. Des.* **2018**, *137*, 79–89. [\[CrossRef\]](#)
160. Shulga, E.; Karamov, R.; Sergeichev, I.S.; Konev, S.D.; Shurygina, L.I.; Akhatov, I.S.; Shandakov, S.D.; Nasibulin, A.G. Fused Filament Fabricated Polypropylene Composite Reinforced by Aligned Glass Fibers. *Materials* **2020**, *13*, 3442. [\[CrossRef\]](#)
161. Sodeifian, G.; Ghaseminejad, S.; Yousefi, A.A. Preparation of Polypropylene/Short Glass Fiber Composite as Fused Deposition Modeling (FDM) Filament. *Results Phys.* **2019**, *12*, 205–222. [\[CrossRef\]](#)
162. Carneiro, O.S.; Silva, A.F.; Gomes, R. Fused Deposition Modeling with Polypropylene. *Mater. Des.* **2015**, *83*, 768–776. [\[CrossRef\]](#)
163. Benal, M.G.M.; GS, P.K.; Tambrallimath, V.; HR, G.; Khan, T.Y.; Rajhi, A.A.; Baig, M.A.A. Influence of Short Glass Fibre Reinforcement on Mechanical Properties of 3D Printed ABS-Based Polymer Composites. *Polymers* **2022**, *14*, 1182.
164. Zhong, W.; Li, F.; Zhang, Z.; Song, L.; Li, Z. Short Fiber Reinforced Composites for Fused Deposition Modeling. *Mater. Sci. Eng. A* **2001**, *301*, 125–130. [\[CrossRef\]](#)
165. Ranganathan, S.; Rangasamy Suguna Thangaraj, H.N.; Vasudevan, A.K.; Shanmugan, D.K. Analogy of Thermal Properties of Polyamide 6 Reinforced with Glass Fiber and Glass Beads through FDM Process. *SAE Tech. Pap. Ser.* **2019**, 1–6. [\[CrossRef\]](#)
166. Luke, S.S.; Soares, D.; Marshall, J.V.; Shedden, J.; Keleş, Ö. Effect of Fiber Content and Fiber Orientation on Mechanical Behavior of Fused Filament Fabricated Continuous-Glass-Fiber-Reinforced Nylon. *Rapid Prototyp. J.* **2021**, *27*, 1346–1354. [\[CrossRef\]](#)
167. Dickson, A.N.; Barry, J.N.; McDonnell, K.A.; Dowling, D.P. Fabrication of Continuous Carbon, Glass and Kevlar Fibre Reinforced Polymer Composites Using Additive Manufacturing. *Addit. Manuf.* **2017**, *16*, 146–152. [\[CrossRef\]](#)

168. Chabaud, G.; Castro, M.; Denoual, C.; Le Duigou, A. Hygromechanical Properties of 3D Printed Continuous Carbon and Glass Fibre Reinforced Polyamide Composite for Outdoor Structural Applications. *Addit. Manuf.* **2019**, *26*, 94–105. [\[CrossRef\]](#)
169. Rahimizadeh, A.; Kalman, J.; Fayazbakhsh, K.; Lessard, L. Recycling of Fiberglass Wind Turbine Blades into Reinforced Filaments for Use in Additive Manufacturing. *Compos. Part B Eng.* **2019**, *175*, 107101. [\[CrossRef\]](#)
170. Li, X.; Ni, Z.; Bai, S.; Lou, B. Preparation and Mechanical Properties of Fiber Reinforced PLA for 3D Printing Materials. *IOP Conf. Ser. Mater. Sci. Eng.* **2018**, *322*, 022012. [\[CrossRef\]](#)
171. Chen, K.; Yu, L.; Cui, Y.; Jia, M.; Pan, K. Optimization of Printing Parameters of 3D-Printed Continuous Glass Fiber Reinforced Polylactic Acid Composites. *Thin-Walled Struct.* **2021**, *164*, 107717. [\[CrossRef\]](#)
172. Akhoundi, B.; Behraves, A.H.; Nabipour, M.; Saed, A.B. Additive manufacturing of glass-fiber reinforced composites using fdm 3d printer. In Proceedings of the 25th Annual International Conference on Mechanical Engineering, Tarbiat Modares University, Tehran, Iran, 2–7 May 2017.
173. Wang, P.; Zou, B.; Ding, S.; Li, L.; Huang, C. Effects of FDM-3D Printing Parameters on Mechanical Properties and Microstructure of CF/PEEK and GF/PEEK. *Chin. J. Aeronaut.* **2020**, *34*, 236–246. [\[CrossRef\]](#)
174. Brown, K.R.; Harrell, T.M.; Skrzypczak, L.; Scherschel, A.; Wu, H.F.; Li, X. Carbon Fibers Derived from Commodity Polymers: A Review. *Carbon* **2022**, *196*, 422–439. [\[CrossRef\]](#)
175. Liu, Y.; Zwingmann, B.; Schlaich, M. Carbon Fiber Reinforced Polymer for Cable Structures—A Review. *Polymers* **2015**, *7*, 2078–2099. [\[CrossRef\]](#)
176. Choi, D.; Kil, H.-S.; Lee, S. Fabrication of Low-Cost Carbon Fibers Using Economical Precursors and Advanced Processing Technologies. *Carbon* **2019**, *142*, 610–649. [\[CrossRef\]](#)
177. Rajak, D.K.; Wagh, P.H.; Linul, E. Manufacturing Technologies of Carbon/Glass Fiber-Reinforced Polymer Composites and Their Properties: A Review. *Polymers* **2021**, *13*, 3721. [\[CrossRef\]](#) [\[PubMed\]](#)
178. El Magri, A.; El Mabrouk, K.; Vaudreuil, S.; Ebn Touhami, M. Mechanical Properties of CF-Reinforced PLA Parts Manufactured by Fused Deposition Modeling. *J. Thermoplast. Compos. Mater.* **2019**, *34*, 581–595. [\[CrossRef\]](#)
179. Ning, F.; Cong, W.; Hu, Y.; Wang, H. Additive Manufacturing of Carbon Fiber-Reinforced Plastic Composites Using Fused Deposition Modeling: Effects of Process Parameters on Tensile Properties. *J. Compos. Mater.* **2016**, *51*, 451–462. [\[CrossRef\]](#)
180. Sanei, S.H.R.; Popescu, D. 3D-Printed Carbon Fiber Reinforced Polymer Composites: A Systematic Review. *J. Compos. Sci.* **2020**, *4*, 98. [\[CrossRef\]](#)
181. Ansari, A.A.; Kamil, M. Izod Impact and Hardness Properties of 3D Printed Lightweight CF-Reinforced PLA Composites Using Design of Experiment. *Int. J. Lightweight Mater. Manuf.* **2022**, *5*, 369–383. [\[CrossRef\]](#)
182. Blanco, I.; Cicala, G.; Recca, G.; Tosto, C. Specific Heat Capacity and Thermal Conductivity Measurements of PLA-Based 3D-Printed Parts with Milled Carbon Fiber Reinforcement. *Entropy* **2022**, *24*, 654. [\[CrossRef\]](#)
183. Bakis, C.E.; Haluza, R.T.; Bartolai, J.; Kim, J.J.; Simpson, T.W. Assessment of Anisotropic Mechanical Properties of a 3D Printed Carbon Whisker Reinforced Composite. *Adv. Compos. Mater.* **2019**, *28*, 545–560. [\[CrossRef\]](#)
184. Ferreira, R.T.L.; Amatte, I.C.; Dutra, T.A.; Bürger, D. Experimental Characterization and Micrography of 3D Printed PLA and PLA Reinforced with Short Carbon Fibers. *Compos. Part B Eng.* **2017**, *124*, 88–100. [\[CrossRef\]](#)
185. Ivey, M.; Melenka, G.W.; Carey, J.P.; Ayranci, C. Characterizing Short-Fiber-Reinforced Composites Produced Using Additive Manufacturing. *Adv. Manuf. Polym. Compos. Sci.* **2017**, *3*, 81–91. [\[CrossRef\]](#)
186. Durga Prasada Rao, V.; Rajiv, P.; Navya Geethika, V. Effect of Fused Deposition Modelling (FDM) Process Parameters on Tensile Strength of Carbon Fibre PLA. *Mater. Today Proc.* **2019**, *18*, 2012–2018. [\[CrossRef\]](#)
187. Al Zahmi, S.; Alhammedi, S.; ElHassan, A.; Ahmed, W. Carbon Fiber/PLA Recycled Composite. *Polymers* **2022**, *14*, 2194. [\[CrossRef\]](#)
188. Vakharia, V.S.; Singh, M.; Salem, A.; Halbig, M.C.; Salem, J.A. Effect of Reinforcements and 3-D Printing Parameters on the Microstructure and Mechanical Properties of Acrylonitrile Butadiene Styrene (ABS) Polymer Composites. *Polymers* **2022**, *14*, 2105. [\[CrossRef\]](#) [\[PubMed\]](#)
189. Tekinalp, H.L.; Kunc, V.; Velez-Garcia, G.M.; Duty, C.E.; Love, L.J.; Naskar, A.K.; Blue, C.A.; Ozcan, S. Highly Oriented Carbon Fiber–Polymer Composites via Additive Manufacturing. *Compos. Sci. Technol.* **2014**, *105*, 144–150. [\[CrossRef\]](#)
190. Ning, F.; Cong, W.; Qiu, J.; Wei, J.; Wang, S. Additive Manufacturing of Carbon Fiber Reinforced Thermoplastic Composites Using Fused Deposition Modeling. *Compos. Part B Eng.* **2015**, *80*, 369–378. [\[CrossRef\]](#)
191. Love, L.J.; Kunc, V.; Rios, O.; Duty, C.E.; Elliott, A.M.; Post, B.K.; Smith, R.J.; Blue, C.A. The Importance of Carbon Fiber to Polymer Additive Manufacturing. *J. Mater. Res.* **2014**, *29*, 1893–1898. [\[CrossRef\]](#)
192. Wang, K.; Li, S.; Rao, Y.; Wu, Y.; Peng, Y.; Yao, S.; Ahzi, S. Flexure Behaviors of ABS-Based Composites Containing Carbon and Kevlar Fibers by Material Extrusion 3D Printing. *Polymers* **2019**, *11*, 1878. [\[CrossRef\]](#)
193. Verdejo de Toro, E.; Coello Sobrino, J.; Martínez Martínez, A.; Miguel Eguía, V.; Ayllón Pérez, J. Investigation of a Short Carbon Fibre-Reinforced Polyamide and Comparison of Two Manufacturing Processes: Fused Deposition Modelling (FDM) and Polymer Injection Moulding (PIM). *Materials* **2020**, *13*, 672. [\[CrossRef\]](#)
194. Chicos, L.-A.; Pop, M.A.; Zaharia, S.-M.; Lancea, C.; Buican, G.R.; Pascariu, I.S.; Stamate, V.-M. Infill Density Influence on Mechanical and Thermal Properties of Short Carbon Fiber-Reinforced Polyamide Composites Manufactured by FFF Process. *Materials* **2022**, *15*, 3706. [\[CrossRef\]](#)

195. Zhang, Z.; Gkartzou, E.; Jestin, S.; Semitekolos, D.; Pappas, P.-N.; Li, X.; Karatza, A.; Zouboulis, P.; Trompeta, A.-F.; Koutroumanis, N.; et al. 3D Printing Processability of a Thermally Conductive Compound Based on Carbon Nanofiller-Modified Thermoplastic Polyamide 12. *Polymers* **2022**, *14*, 470. [\[CrossRef\]](#) [\[PubMed\]](#)
196. Imeri, A.; Fidan, I.; Allen, M.; Wilson, D.A.; Canfield, S. Fatigue Analysis of the Fiber Reinforced Additively Manufactured Objects. *Int. J. Adv. Manuf. Technol.* **2018**, *98*, 2717–2724. [\[CrossRef\]](#)
197. Justo, J.; Távara, L.; García-Guzmán, L.; París, F. Characterization of 3D Printed Long Fibre Reinforced Composites. *Compos. Struct.* **2018**, *185*, 537–548. [\[CrossRef\]](#)
198. Kováčová, M.; Kozakovičová, J.; Procházka, M.; Janigová, I.; Vysopal, M.; Černíková, I.; Krajčovič, J.; Špitalský, Z. Novel Hybrid PETG Composites for 3D Printing. *Appl. Sci.* **2020**, *10*, 3062. [\[CrossRef\]](#)
199. Ferreira, I.; Vale, D.; Machado, M.; Lino, J. Additive Manufacturing of Polyethylene Terephthalate Glycol/Carbon Fiber Composites: An Experimental Study from Filament to Printed Parts. *Proc. Inst. Mech. Eng. Part L J. Mater. Des. Appl.* **2018**, *233*, 1866–1878. [\[CrossRef\]](#)
200. Valvez, S.; Silva, A.P.; Reis, P.N.B. Optimization of Printing Parameters to Maximize the Mechanical Properties of 3D-Printed PETG-Based Parts. *Polymers* **2022**, *14*, 2564. [\[CrossRef\]](#)
201. Valvez, S.; Silva, A.P.; Reis, P.N.B. Compressive Behaviour of 3D-Printed PETG Composites. *Aerospace* **2022**, *9*, 124. [\[CrossRef\]](#)
202. Mansour, M.; Tsongas, K.; Tzetzis, D.; Antoniadis, A. Mechanical and Dynamic Behavior of Fused Filament Fabrication 3D Printed Polyethylene Terephthalate Glycol Reinforced with Carbon Fibers. *Polym.-Plast. Technol. Eng.* **2018**, *57*, 1715–1725. [\[CrossRef\]](#)
203. Wang, P.; Zou, B.; Ding, S.; Huang, C.; Shi, Z.; Ma, Y.; Yao, P. Preparation of Short CF/GF Reinforced PEEK Composite Filaments and Their Comprehensive Properties Evaluation for FDM-3D Printing. *Compos. Part B Eng.* **2020**, *198*, 108175. [\[CrossRef\]](#)
204. Patterson, A.E.; Pereira, T.R.; Allison, J.T.; Messimer, S.L. IZOD Impact Properties of Full-Density Fused Deposition Modeling Polymer Materials with Respect to Raster Angle and Print Orientation. *Proc. Inst. Mech. Eng. Part C J. Mech. Eng. Sci.* **2019**, *235*, 1891–1908. [\[CrossRef\]](#)
205. Gupta, A.; Fidan, I.; Hasanov, S.; Nasirov, A. Processing, Mechanical Characterization, and Micrography of 3D-Printed Short Carbon Fiber Reinforced Polycarbonate Polymer Matrix Composite Material. *Int. J. Adv. Manuf. Technol.* **2020**, *107*, 3185–3205. [\[CrossRef\]](#)
206. Lamin, W.M.; Bussamra, F.L.; Ferreira, R.T.; Sales, R.C.; Baldo, J.E. Linear Translaminar Fracture Characterization of Additive Manufactured Continuous Carbon Fiber Reinforced Thermoplastic. *J. Thermoplast. Compos. Mater.* **2021**, 1–28. [\[CrossRef\]](#)
207. Hu, Q.; Duan, Y.; Zhang, H.; Liu, D.; Yan, B.; Peng, F. Manufacturing and 3D Printing of Continuous Carbon Fiber Prepreg Filament. *J. Mater. Sci.* **2017**, *53*, 1887–1898. [\[CrossRef\]](#)
208. Hao, W.; Liu, Y.; Zhou, H.; Chen, H.; Fang, D. Preparation and Characterization of 3D Printed Continuous Carbon Fiber Reinforced Thermosetting Composites. *Polym. Test.* **2018**, *65*, 29–34. [\[CrossRef\]](#)
209. Luo, M.; Tian, X.; Shang, J.; Zhu, W.; Li, D.; Qin, Y. Impregnation and Interlayer Bonding Behaviours of 3D-Printed Continuous Carbon-Fiber-Reinforced Poly-Ether-Ether-Ketone Composites. *Compos. Part A Appl. Sci. Manuf.* **2019**, *121*, 130–138. [\[CrossRef\]](#)
210. Yu, T.; Zhang, Z.; Song, S.; Bai, Y.; Wu, D. Tensile and Flexural Behaviors of Additively Manufactured Continuous Carbon Fiber-Reinforced Polymer Composites. *Compos. Struct.* **2019**, *225*, 111147. [\[CrossRef\]](#)
211. Wu, Y.; Wang, K.; Neto, V.; Peng, Y.; Valente, R.; Ahzi, S. Interfacial Behaviors of Continuous Carbon Fiber Reinforced Polymers Manufactured by Fused Filament Fabrication: A Review and Prospect. *Int. J. Mater. Form.* **2022**, *15*, 18. [\[CrossRef\]](#)
212. Blok, L.G.; Longana, M.L.; Yu, H.; Woods, B.K.S. An Investigation into 3D Printing of Fibre Reinforced Thermoplastic Composites. *Addit. Manuf.* **2018**, *22*, 176–186. [\[CrossRef\]](#)
213. Sang, L.; Han, S.; Li, Z.; Yang, X.; Hou, W. Development of short basalt fiber reinforced polylactide composites and their feasible evaluation for 3D printing applications. *Compos. Part B Eng.* **2019**, *164*, 629–639. [\[CrossRef\]](#)
214. Sang, L.; Han, S.; Peng, X.; Jian, X.; Wang, J. Development of 3D-printed basalt fiber reinforced thermoplastic honeycombs with enhanced compressive mechanical properties. *Compos. Part A Appl. Sci. Manuf.* **2019**, *125*, 105518. [\[CrossRef\]](#)
215. Yu, S.; Bale, H.; Park, S.; Hwang, J.Y.; Hong, S.H. Anisotropic microstructure dependent mechanical behavior of 3D-printed basalt fiber-reinforced thermoplastic composites. *Compos. Part B Eng.* **2021**, *224*, 109184. [\[CrossRef\]](#)
216. Yu, S.; Hwang, Y.H.; Hwang, J.Y.; Hong, S.H. Analytical Study on the 3D-Printed Structure and Mechanical Properties of Basalt Fiber-Reinforced PLA Composites Using X-Ray Microscopy. *Compos. Sci. Technol.* **2019**, *175*, 18–27. [\[CrossRef\]](#)
217. Kurniawan, D.; Kim, B.S.; Lee, H.Y.; Lim, J.Y. Towards improving mechanical properties of basalt fiber/polylactic acid composites by fiber surface treatments. *Compos. Interfaces* **2015**, *22*, 553–562. [\[CrossRef\]](#)
218. Balaji, K.V.; Shirvanimoghaddam, K.; Rajan, G.S.; Ellis, A.V.; Naebe, M. Surface treatment of Basalt fiber for use in automotive composites. *Mater. Today Chem.* **2020**, *17*, 100334.
219. Zotti, A.; Zuppolini, S.; Tábi, T.; Grasso, M.; Ren, G.; Borriello, A.; Zarrelli, M. Effects of 1D and 2D Nanofillers in Basalt/Poly(Lactic Acid) Composites for Additive Manufacturing. *Compos. Part B Eng.* **2018**, *153*, 364–375. [\[CrossRef\]](#)
220. Arslan, C.; Dogan, M. Effect of fiber amount on mechanical and thermal properties of (3-aminopropyl) triethoxysilane treated basalt fiber reinforced ABS composites. *Mater. Res. Express* **2019**, *6*, 115340. [\[CrossRef\]](#)
221. Coughlin, N.; Drake, B.; Fjerstad, M.; Schuster, E.; Waage, T.; Weerakkody, A.; Letcher, T. Development and mechanical properties of basalt fiber-reinforced acrylonitrile butadiene styrene for in-space manufacturing applications. *J. Compos. Sci.* **2019**, *3*, 89. [\[CrossRef\]](#)

222. Dowling, D.P.; Abourayana, H.M.; Brantseva, T.; Antonov, A.; Dobbyn, P.J. Enhancing the mechanical performance of 3D-printed basalt fiber-reinforced composites using in-line atmospheric plasma pretreatments. *Plasma Process. Polym.* **2020**, *17*, 1900143. [[CrossRef](#)]
223. Bailly, M.; Kontopoulou, M.; El Mabrouk, K. Effect of Polymer/Filler Interactions on the Structure and Rheological Properties of Ethylene-Octene Copolymer/Nanosilica Composites. *Polymer* **2010**, *51*, 5506–5515. [[CrossRef](#)]
224. Babanzadeh, S.; Mehdipour-Ataei, S.; Mahjoub, A.R. Effect of Nanosilica on the Dielectric Properties and Thermal Stability of Polyimide/SiO₂Nanohybrid. *Des. Monomers Polym.* **2012**, *16*, 417–424. [[CrossRef](#)]
225. Wu, G.; Liu, S.; Jia, H.; Dai, J. Preparation and Properties of Heat Resistant Polylactic Acid (PLA)/Nano-SiO₂ Composite Filament. *J. Wuhan Univ. Technol.-Mater. Sci. Ed.* **2016**, *31*, 164–171. [[CrossRef](#)]
226. Gong, Z.; Huang, J.; Fan, J.; Chen, X.; Wang, H.; Chen, Y. A Super-Toughened Poly(Lactic Acid)-Based Thermoplastic Vulcanizate through Incorporating Modified SiO₂ Nanoparticles. *Compos. Sci. Technol.* **2022**, *226*, 109558. [[CrossRef](#)]
227. Gong, Z.; Huang, J.; Fan, J.; Chen, X.; Wang, H.; Chen, Y. Super-Tough Poly(Lactic Acid)-Based Thermoplastic Vulcanizate Based on Selective Dispersion and in Situ Compatibilization of Commercial Reinforcing Fillers and Its Application in Three-Dimensional Printing. *Ind. Eng. Chem. Res.* **2021**, *61*, 359–371. [[CrossRef](#)]
228. Kodali, D.; Umerah, C.O.; Idrees, M.O.; Jeelani, S.; Rangari, V.K. Fabrication and Characterization of Polycarbonate-Silica Filaments for 3D Printing Applications. *J. Compos. Mater.* **2021**, *55*, 4575–4584. [[CrossRef](#)]
229. Ramachandran, M.G.; Rajeswari, N. Influence of Nano Silica on Mechanical and Tribological Properties of Additive Manufactured PLA Bio Nanocomposite. *Silicon* **2021**, *14*, 703–709. [[CrossRef](#)]
230. Sharma, A.; Singholi, A.K.S. Effect of Nanosilica on Shape Memory and Mechanical Characterization of Polylactic Acid Wood Composite. *Polym. Compos.* **2021**, *42*, 2502–2510. [[CrossRef](#)]
231. Sharma, A.; Singholi, A.K.S. Shape Memory and Mechanical Characterization of Polylactic Acid Wood Composite Fabricated by Fused Filament Fabrication 4D Printing Technology. *Mater. Und Werkst.* **2021**, *52*, 635–643. [[CrossRef](#)]
232. Seng, C.T.; A/L Eh Noum, S.Y.; A/L Sivanesan, S.K.; Yu, L.-J. Reduction of Hygroscopicity of PLA Filament for 3D Printing by Introducing Nano Silica as Filler. In Proceedings of the 13th International Engineering Research Conference 13th Eureka 2019, Selangor Darul Ehsan, Malaysia, 27 November 2019.
233. Vidakis, N.; Petousis, M.; Velidakis, E.; Tzounis, L.; Mountakis, N.; Korlos, A.; Fischer-Griffiths, P.E.; Grammatikos, S. On the Mechanical Response of Silicon Dioxide Nanofiller Concentration on Fused Filament Fabrication 3D Printed Isotactic Polypropylene Nanocomposites. *Polymers* **2021**, *13*, 2029. [[CrossRef](#)]
234. Vidakis, N.; Petousis, M.; Velidakis, E.; Mountakis, N.; Tzounis, L.; Liebscher, M.; Grammatikos, S.A. Enhanced Mechanical, Thermal and Antimicrobial Properties of Additively Manufactured Polylactic Acid with Optimized Nano Silica Content. *Nanomaterials* **2021**, *11*, 1012. [[CrossRef](#)]
235. Novoselov, K.S. Electric Field Effect in Atomically Thin Carbon Films. *Science* **2004**, *306*, 666–669. [[CrossRef](#)]
236. Joudeh, N.; Linke, D. Nanoparticle Classification, Physicochemical Properties, Characterization, and Applications: A Comprehensive Review for Biologists. *J. Nanobiotechnol.* **2022**, *20*, 1–29. [[CrossRef](#)] [[PubMed](#)]
237. Farmand, M.; Jahanpeyma, F.; Gholaminejad, A.; Azimzadeh, M.; Malaee, F.; Shoaie, N. Carbon Nanostructures: A Comprehensive Review of Potential Applications and Toxic Effects. *3 Biotech* **2022**, *12*, 159. [[CrossRef](#)] [[PubMed](#)]
238. Park, S.; Fu, K. Polymer-Based Filament Feedstock for Additive Manufacturing. *Compos. Sci. Technol.* **2021**, *213*, 108876. [[CrossRef](#)]
239. Foster, C.W.; Down, M.P.; Zhang, Y.; Ji, X.; Rowley-Neale, S.J.; Smith, G.C.; Kelly, P.J.; Banks, C.E. 3D Printed Graphene Based Energy Storage Devices. *Sci. Rep.* **2017**, *7*, 42233. [[CrossRef](#)]
240. Bustillos, J.; Montero, D.; Nautiyal, P.; Loganathan, A.; Boesl, B.; Agarwal, A. Integration of Graphene in Poly(Lactic) Acid by 3D Printing to Develop Creep and Wear-Resistant Hierarchical Nanocomposites. *Polym. Compos.* **2017**, *39*, 3877–3888. [[CrossRef](#)]
241. Caminero, M.Á.; Chacón, J.M.; García-Plaza, E.; Núñez, P.J.; Reverte, J.M.; Becar, J.P. Additive Manufacturing of PLA-Based Composites Using Fused Filament Fabrication: Effect of Graphene Nanoplatelet Reinforcement on Mechanical Properties, Dimensional Accuracy and Texture. *Polymers* **2019**, *11*, 799. [[CrossRef](#)]
242. Sweeney, C.B.; Lackey, B.A.; Pospisil, M.J.; Achee, T.C.; Hicks, V.K.; Moran, A.G.; Teipel, B.R.; Saed, M.A.; Green, M.J. Welding of 3D-Printed Carbon Nanotube–Polymer Composites by Locally Induced Microwave Heating. *Sci. Adv.* **2017**, *3*, e1700262. [[CrossRef](#)]
243. Ivanov, E.; Kotsilkova, R.; Xia, H.; Chen, Y.; Donato, R.; Donato, K.; Godoy, A.; Di Maio, R.; Silvestre, C.; Cimmino, S.; et al. PLA/Graphene/MWCNT Composites with Improved Electrical and Thermal Properties Suitable for FDM 3D Printing Applications. *Appl. Sci.* **2019**, *9*, 1209. [[CrossRef](#)]
244. Foo, C.Y.; Lim, H.N.; Mahdi, M.A.; Wahid, M.H.; Huang, N.M. Three-Dimensional Printed Electrode and Its Novel Applications in Electronic Devices. *Sci. Rep.* **2018**, *8*, 7399. [[CrossRef](#)]
245. Chen, Q.; Mangadlao, J.D.; Wallat, J.; De Leon, A.; Pokorski, J.K.; Advincula, R.C. 3D Printing Biocompatible Polyurethane/Poly(Lactic Acid)/Graphene Oxide Nanocomposites: Anisotropic Properties. *ACS Appl. Mater. Interfaces* **2017**, *9*, 4015–4023. [[CrossRef](#)]
246. Kim, K.; Park, J.; Suh, J.; Kim, M.; Jeong, Y.; Park, I. 3D Printing of Multiaxial Force Sensors Using Carbon Nanotube (CNT)/Thermoplastic Polyurethane (TPU) Filaments. *Sens. Actuators A Phys.* **2017**, *263*, 493–500. [[CrossRef](#)]
247. Christ, J.F.; Aliheidari, N.; Ameli, A.; Pötschke, P. 3D Printed Highly Elastic Strain Sensors of Multiwalled Carbon Nanotube/Thermoplastic Polyurethane Nanocomposites. *Mater. Des.* **2017**, *131*, 394–401. [[CrossRef](#)]

248. Xiang, D.; Zhang, X.; Li, Y.; Harkin-Jones, E.; Zheng, Y.; Wang, L.; Zhao, C.; Wang, P. Enhanced Performance of 3D Printed Highly Elastic Strain Sensors of Carbon Nanotube/Thermoplastic Polyurethane Nanocomposites via Non-Covalent Interactions. *Compos. Part B Eng.* **2019**, *176*, 107250. [[CrossRef](#)]
249. Podsiadły, B.; Matuszewski, P.; Skalski, A.; Słoma, M. Carbon Nanotube-Based Composite Filaments for 3D Printing of Structural and Conductive Elements. *Appl. Sci.* **2021**, *11*, 1272. [[CrossRef](#)]
250. Sezer, H.K.; Eren, O. FDM 3D Printing of MWCNT Re-Inforced ABS Nano-Composite Parts with Enhanced Mechanical and Electrical Properties. *J. Manuf. Process.* **2019**, *37*, 339–347. [[CrossRef](#)]
251. Dorigato, A.; Moretti, V.; Dul, S.; Unterberger, S.H.; Pegoretti, A. Electrically Conductive Nanocomposites for Fused Deposition Modelling. *Synth. Met.* **2017**, *226*, 7–14. [[CrossRef](#)]
252. Shofner, M.L.; Rodríguez-Macías, F.J.; Vaidyanathan, R.; Barrera, E.V. Single Wall Nanotube and Vapor Grown Carbon Fiber Reinforced Polymers Processed by Extrusion Freeform Fabrication. *Compos. Part A Appl. Sci. Manuf.* **2003**, *34*, 1207–1217. [[CrossRef](#)]
253. Wei, X.; Li, D.; Jiang, W.; Gu, Z.; Wang, X.; Zhang, Z.; Sun, Z. 3D Printable Graphene Composite. *Sci. Rep.* **2015**, *5*, 11181. [[CrossRef](#)]
254. Dul, S.; Fambri, L.; Pegoretti, A. Fused Deposition Modelling with ABS–Graphene Nanocomposites. *Compos. Part A Appl. Sci. Manuf.* **2016**, *85*, 181–191. [[CrossRef](#)]
255. Singh, R.; Singh, H.; Farina, I.; Colangelo, F.; Fraternali, F. On the Additive Manufacturing of an Energy Storage Device from Recycled Material. *Compos. Part B Eng.* **2019**, *156*, 259–265. [[CrossRef](#)]
256. Aumtate, C.; Pongwisuthiruchte, A.; Pattanauwat, P.; Potiyaraj, P. Fabrication of ABS/Graphene Oxide Composite Filament for Fused Filament Fabrication (FFF) 3D Printing. *Adv. Mater. Sci. Eng.* **2018**, *2018*, 2830437. [[CrossRef](#)]
257. Zhang, J.; Yang, B.; Fu, F.; You, F.; Dong, X.; Dai, M. Resistivity and Its Anisotropy Characterization of 3D-Printed Acrylonitrile Butadiene Styrene Copolymer (ABS)/Carbon Black (CB) Composites. *Appl. Sci.* **2017**, *7*, 20. [[CrossRef](#)]
258. Berretta, S.; Davies, R.; Shyng, Y.T.; Wang, Y.; Ghita, O. Fused Deposition Modelling of High Temperature Polymers: Exploring CNT PEEK Composites. *Polym. Test.* **2017**, *63*, 251–262. [[CrossRef](#)]
259. Gonçalves, J.; Lima, P.; Krause, B.; Pötschke, P.; Lafont, U.; Gomes, J.; Abreu, C.; Paiva, M.; Covas, J. Electrically Conductive Polyetheretherketone Nanocomposite Filaments: From Production to Fused Deposition Modeling. *Polymers* **2018**, *10*, 925. [[CrossRef](#)]
260. Zhu, D.; Ren, Y.; Liao, G.; Jiang, S.; Liu, F.; Guo, J.; Xu, G. Thermal and Mechanical Properties of Polyamide 12/Graphene Nanoplatelets Nanocomposites and Parts Fabricated by Fused Deposition Modeling. *J. Appl. Polym. Sci.* **2017**, *134*, 45332. [[CrossRef](#)]
261. Han, J.Y.; Chen, T.; Baird, D.G. Generation of Nylon Copolymer Reinforced with Carbon Nanotubes and Thermotropic Liquid Crystalline Polymers for Use in Fused Filament Fabrication. *Polym. Compos.* **2021**, *42*, 4328–4341. [[CrossRef](#)]
262. Gnanasekaran, K.; Heijmans, T.; van Bennekom, S.; Woldhuis, H.; Wijnia, S.; de With, G.; Friedrich, H. 3D Printing of CNT- and Graphene-Based Conductive Polymer Nanocomposites by Fused Deposition Modeling. *Appl. Mater. Today* **2017**, *9*, 21–28. [[CrossRef](#)]
263. Kwok, S.W.; Goh, K.H.H.; Tan, Z.D.; Tan, S.T.M.; Tjiu, W.W.; Soh, J.Y.; Ng, Z.J.G.; Chan, Y.Z.; Hui, H.K.; Goh, K.E.J. Electrically Conductive Filament for 3D-Printed Circuits and Sensors. *Appl. Mater. Today* **2017**, *9*, 167–175. [[CrossRef](#)]
264. Han, J.Y.; Chen, T.; Mu, Q.; Baird, D.G. Thermotropic Liquid Crystalline Polymer Reinforced Polypropylene Composites Enhanced with Carbon Nanotubes for Use in Fused Filament Fabrication. *Polym. Compos.* **2021**, *42*, 4115–4127. [[CrossRef](#)]
265. Kennedy, Z.C.; Christ, J.F.; Evans, K.A.; Arey, B.W.; Sweet, L.E.; Warner, M.G.; Erikson, R.L.; Barrett, C.A. 3D-Printed Poly(Vinylidene Fluoride)/Carbon Nanotube Composites as a Tunable, Low-Cost Chemical Vapour Sensing Platform. *Nanoscale* **2017**, *9*, 5458–5466. [[CrossRef](#)]
266. Yang, L.; Chen, Y.; Wang, M.; Shi, S.; Jing, J. Fused Deposition Modeling 3D Printing of Novel Poly(Vinyl Alcohol)/Graphene Nanocomposite with Enhanced Mechanical and Electromagnetic Interference Shielding Properties. *Ind. Eng. Chem. Res.* **2020**, *59*, 8066–8077. [[CrossRef](#)]
267. Kumar, N.; Jain, P.K.; Tandon, P.; Pandey, P.M. Additive Manufacturing of Flexible Electrically Conductive Polymer Composites via CNC-Assisted Fused Layer Modeling Process. *J. Braz. Soc. Mech. Sci. Eng.* **2018**, *40*, 175. [[CrossRef](#)]
268. Castles, F.; Isakov, D.; Lui, A.; Lei, Q.; Dancer, C.E.J.; Wang, Y.; Grant, P.S. Microwave dielectric characterisation of 3D-printed BaTiO₃/ABS polymer composites. *Sci. Rep.* **2016**, *6*, 22714. [[CrossRef](#)] [[PubMed](#)]
269. Khatri, B.; Lappe, K.; Habedank, M.; Mueller, T.; Megnin, C.; Hanemann, T. Fused Deposition Modeling of ABS-Barium Titanate Composites: A Simple Route towards Tailored Dielectric Devices. *Polymers* **2018**, *10*, 666. [[CrossRef](#)] [[PubMed](#)]
270. Malakooti, M.H.; Julé, F.; Sodano, H.A. Printed Nanocomposite Energy Harvesters with Controlled Alignment of Barium Titanate Nanowires. *ACS Appl. Mater. Interfaces* **2018**, *10*, 38359–38367. [[CrossRef](#)]
271. Kim, H.; Fernando, T.; Li, M.; Lin, Y.; Tseng, T.-L.B. Fabrication and characterization of 3D printed BaTiO₃/PVDF nanocomposites. *J. Compos. Mater.* **2017**, *52*, 197–206. [[CrossRef](#)]
272. Kim, H.; Torres, F.; Villagran, D.; Stewart, C.; Lin, Y.; Tseng, T.L.B. 3D printing of BaTiO₃/PVDF composites with electric in situ poling for pressure sensor applications. *Macromol. Mater. Eng.* **2017**, *302*, 1700229. [[CrossRef](#)]

-
273. Paspali, A.; Bao, Y.; Gawne, D.T.; Piester, F.; Reinelt, S. The influence of nanostructure on the mechanical properties of 3D printed polylactide/nanoclay composites. *Compos. Part B Eng.* **2018**, *152*, 160–168. [[CrossRef](#)]
 274. Lee, C.H.; Yeoh, C.K.; Hamzah, K.A.; Teh, P.L. Mechanical Properties of Copper Ferrite CuFe₂O₄-Polymer Composite Fabricated Using 3D Printer. *Mater. Sci. Forum* **2017**, *888*, 203–208. [[CrossRef](#)]